RESULTS OF VARIOUS STUDIES MADE WITH THE NCAR THERMOSPHERIC GENERAL CIRCULATION MODEL (TGCM)
(Invited Review)

R. G. Roble
High Altitude Observatory
National Center for Atmospheric Research
Boulder, CO 80307

The NCAR thermospheric general circulation model has been used for a variety of thermospheric dynamic studies. It has also been used to compare model predictions with measurements made from various ground-based Fabry-Perot interferometer stations, incoherent scatter radar stations and the Dynamics Explorer satellites. In this report the various input and output features of the model are described. These include the specification of solar EUV fluxes, and descriptions of empirical models to specify auroral particle precipitation, ion drag, and magnetospheric convection. Results are presented for solstice conditions giving the model perturbation temperature and circulation response to solar heating forcing alone and also with the inclusion of magnetospheric convections for two different dawn-dusk potential drops, 20 and 60 kV respectively. Results at two constant pressure levels Z = +1 at 300 km and Z = -4 at 120 km are presented for both the winter and summer polar cap regions. The circulation over the northern hemisphere polar cap in both the upper and lower thermosphere are presented along with a figure showing that the circulation is mainly a non-divergent irrotational flow responding to ion drag.

The results of a study made on the southern hemisphere polar cap during October 1981 where Dynamics Explorer satellite measurements of winds, temperature and composition are compared to TGCM predictions are also presented. A diagnostic package that has been developed to analyze the balance of forces operating in the TGCM is presented next illustrating that in the F-region ion drag and pressure provide the main force balance and in the E-region ion drag, pressure and the coriolis forces provide the main balance. The TGCM prediction for the June 10, 1983 total solar eclipse are next presented showing a thermospheric disturbance following the path of totality. Finally, results are presented giving the global circulation, temperature and composition structure of the thermosphere for solar minimum conditions at equinox with 60 kV magnetospheric convection forcing at high latitudes.

THERMOSPHERIC GENERAL CIRCULATION MODELS (TGCM)

OUTPUT

- NEUTRAL TEMPERATURE, T_n
- NEUTRAL WINDS u, v, w
- HEIGHT OF CONSTANT PRESSURE SURFACE, h
- NEUTRAL COMPOSITION, $n(O)$, $n(O_2)$, $n(N_2)$

INPUT

- EMPIRICAL ELECTRON DENSITY MODEL
- EMPIRICAL MAGNETIC FIELD
- EMPIRICAL ION DRIFT - MAGNETOSPHERIC CONVECTION
  - WIND DYNAMO
  - COROTATION
- EMPIRICAL AURORAL IONIZATION SOURCE
- OTHER HEAT AND MOMENTUM SOURCES (i.e., PLASMA PAUSE HEATING, EQUATORIAL HEATING, ETC.)

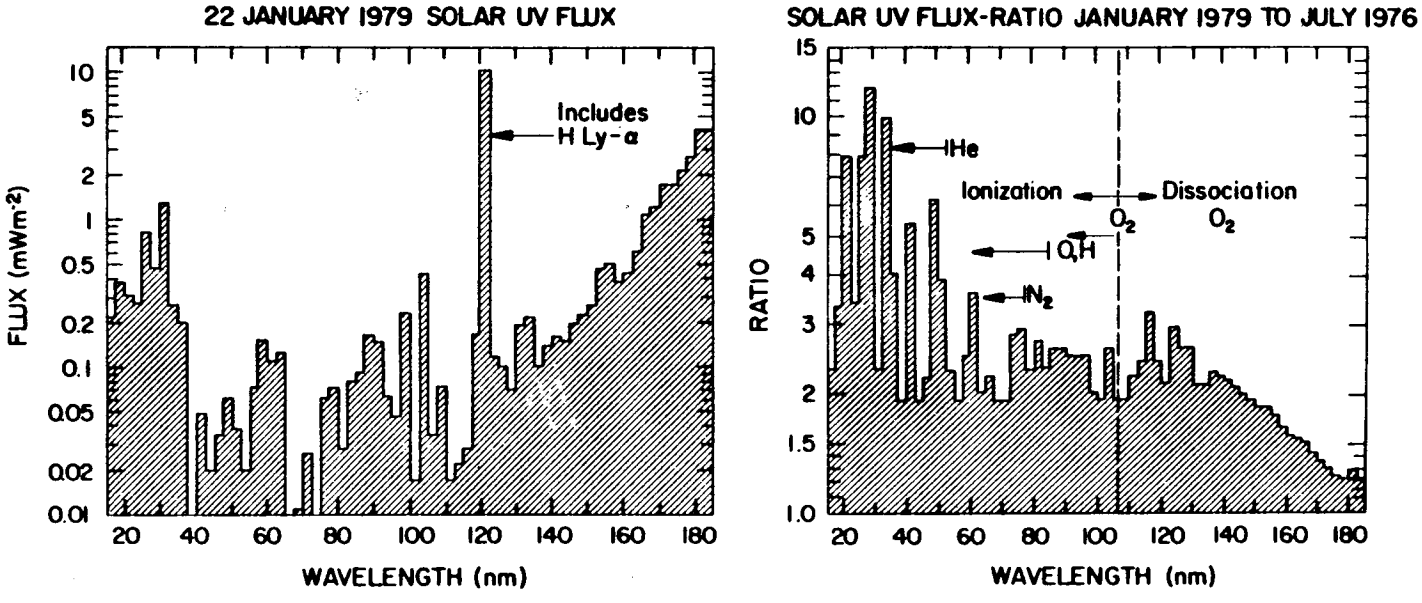

Figure 1. Solar EUV spectrum measured by H. E. Hinteregger from the Atmospheric Explorer satellite on 22 January 1979 and ratio of the Solar EUV flux measured in January 1979 to that on July 1976.

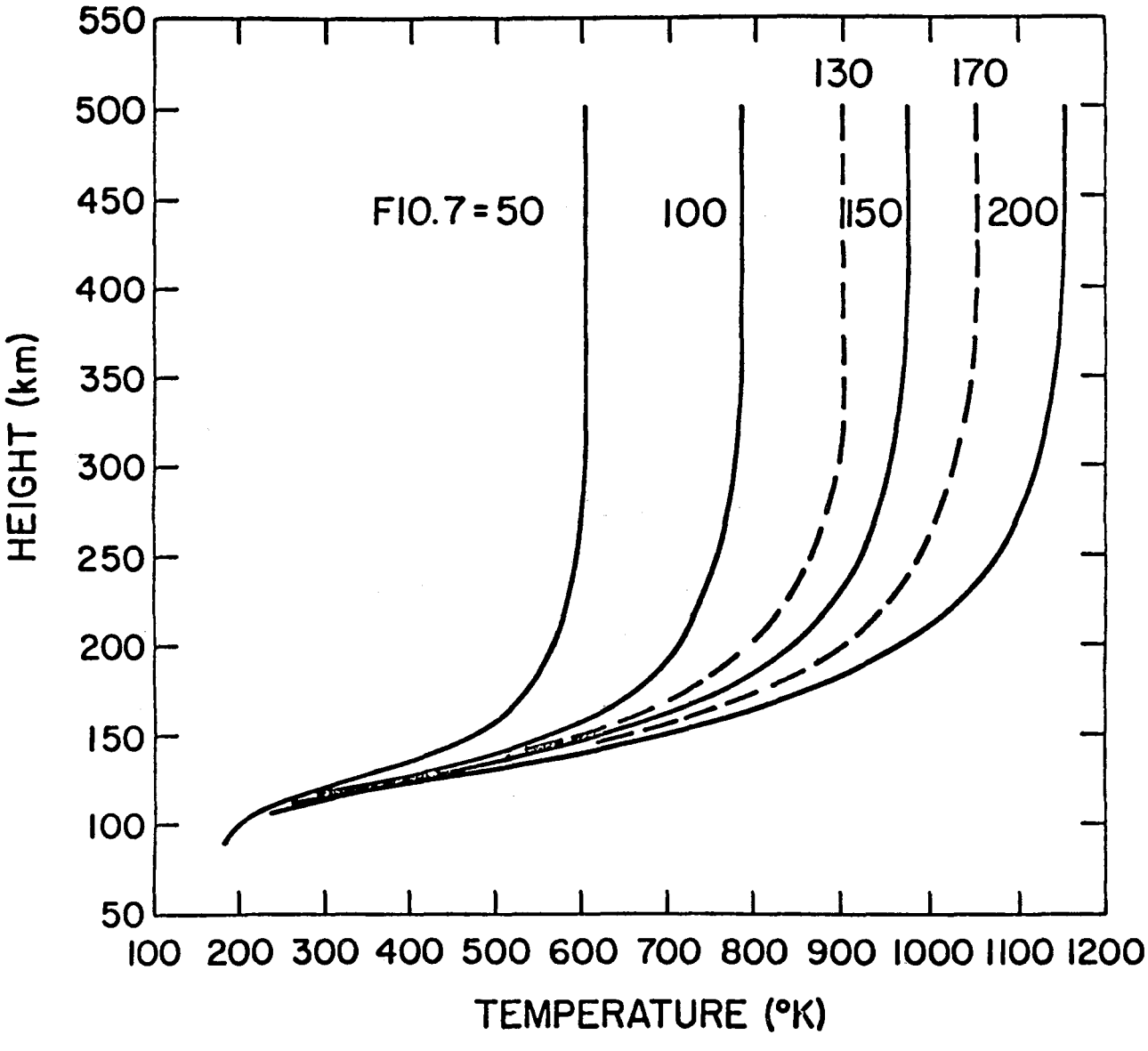

Figure 2. Calculated global mean exospheric temperature profiles for various solar F10.7 values. The dashed lines are predictions from the MSIS model.

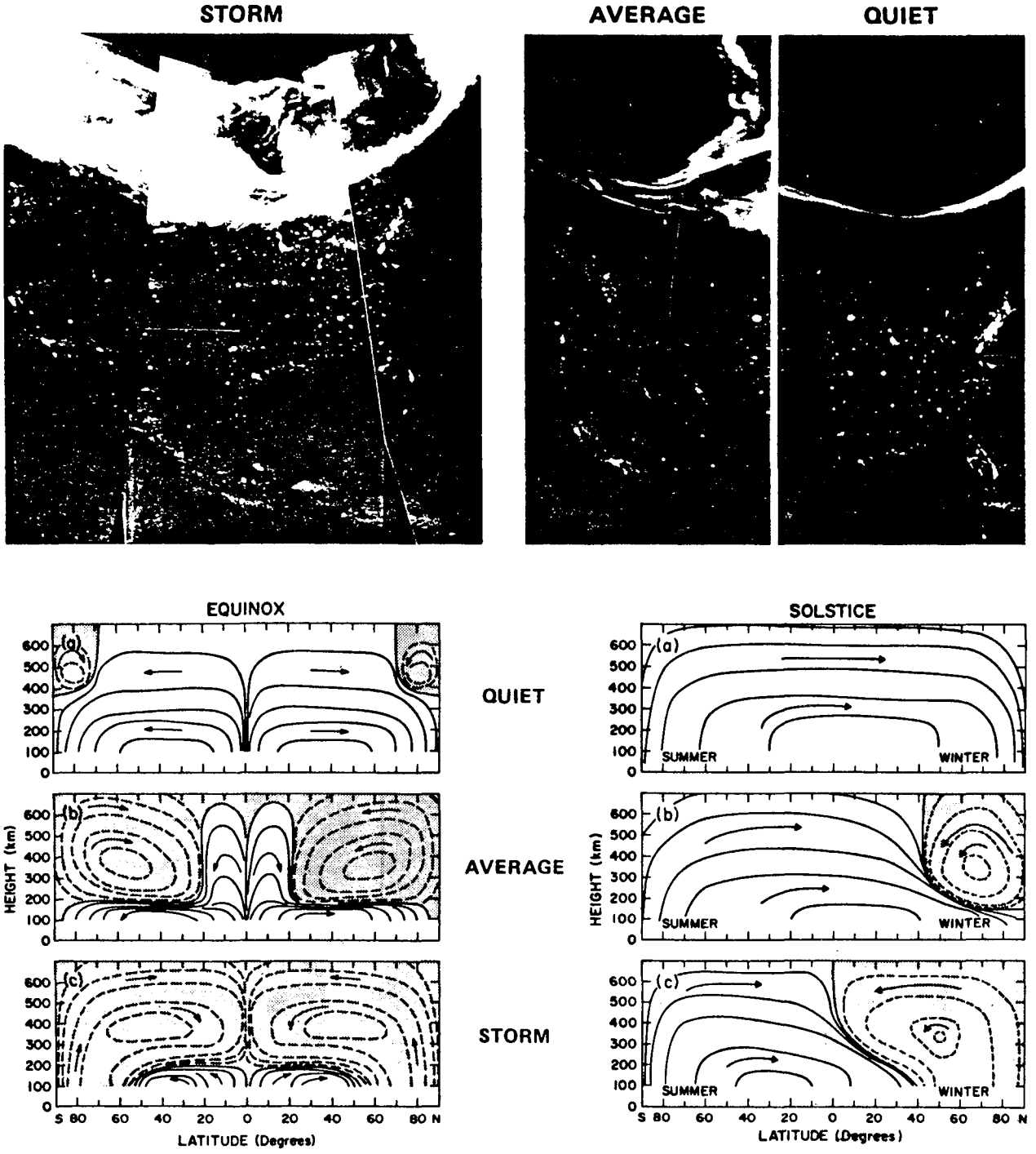

Figure 3. Mean thermospheric circulation for equinox and solstice conditions for various levels of geomagnetic activity.

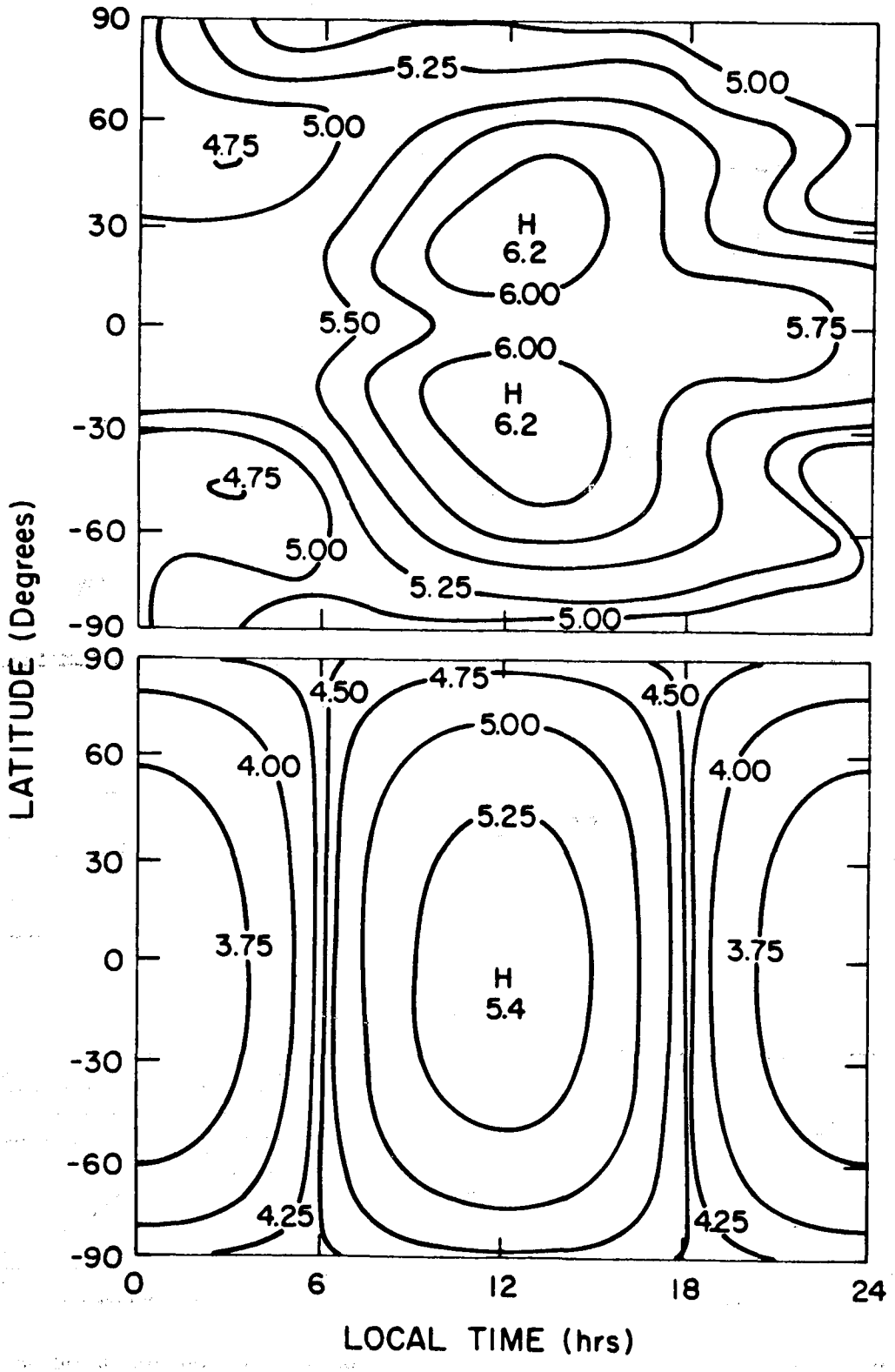

Figure 4. Contours of $\log_{10}$ (n_e, cm^{-3}) the electron densities obtained form the Chiu (1975) model for low solar activity, upper panel at 300 km, lower panel at 120 km.

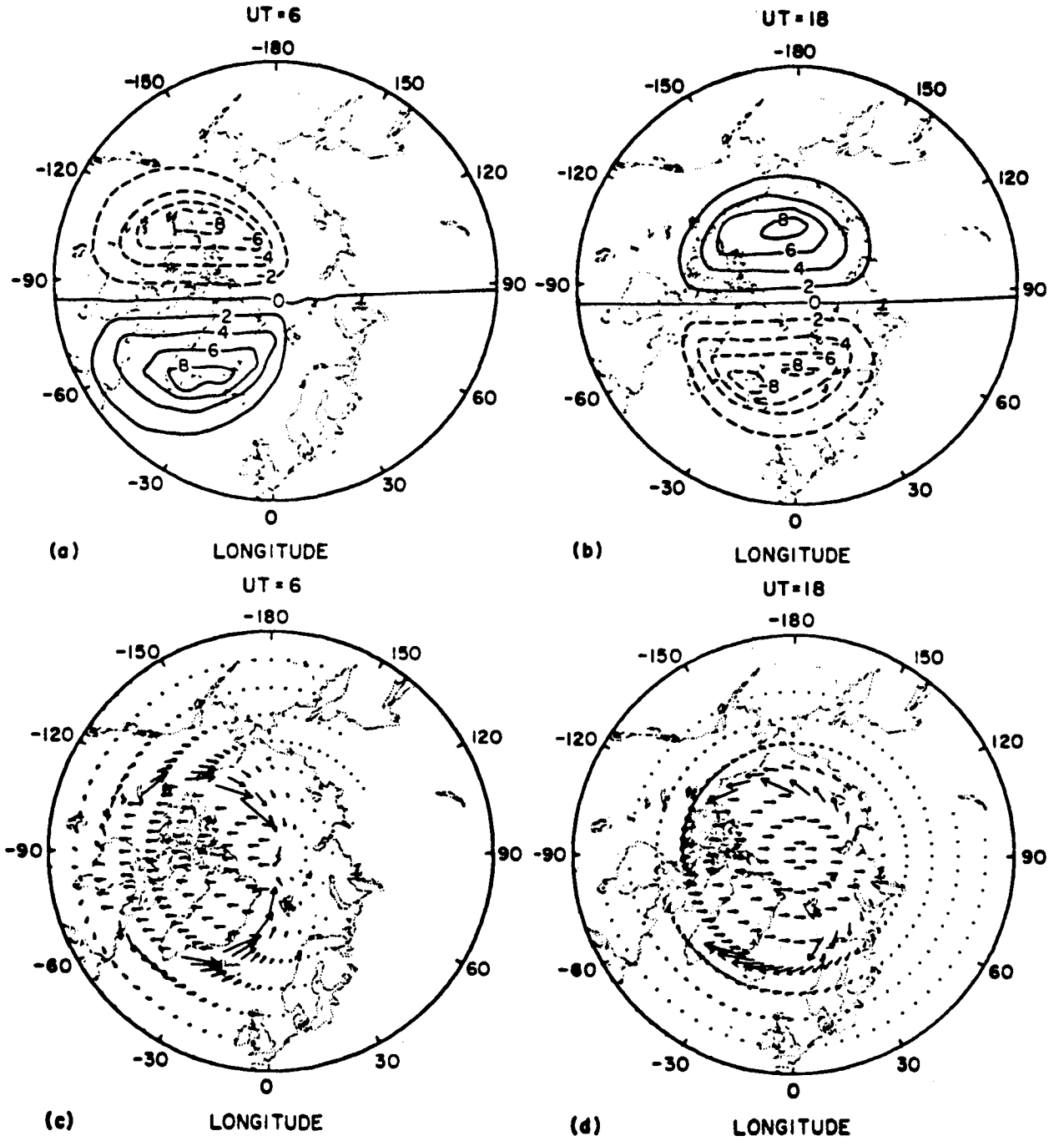

Figure 5. Upper figures, the magnetospheric convection potential pattern in kV for quiet geomagnetic activity over the northern hemisphere polar cap for two UT's. The lower figures represent the direction of the ion drift (E x B) associated with the potential pattern. Max. arrow represents a speed of 375 m s^{-1}.

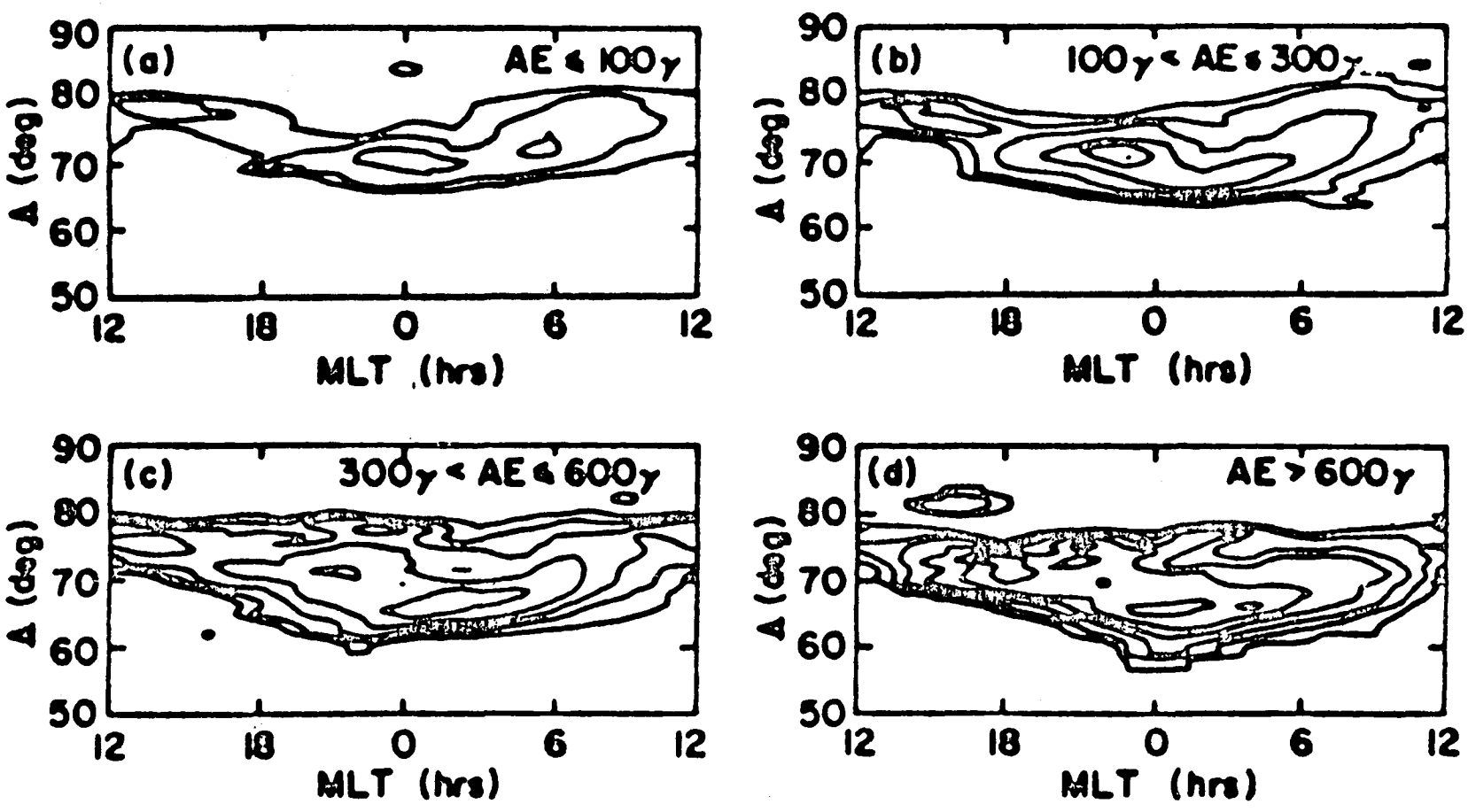

Figure 6. Contours of constant precipitating electron energy flux measured by the Atmospheric Explorer satellite and sorted according to auroral electrojet (AE) index. The outermost contours correspond to a line-average energy flux of 2.5 x 10^{-1} erg cm^{-2} s^{-1}, with adjacent contours representing factor of two increases in energy flux (Spiro et al., 1982)

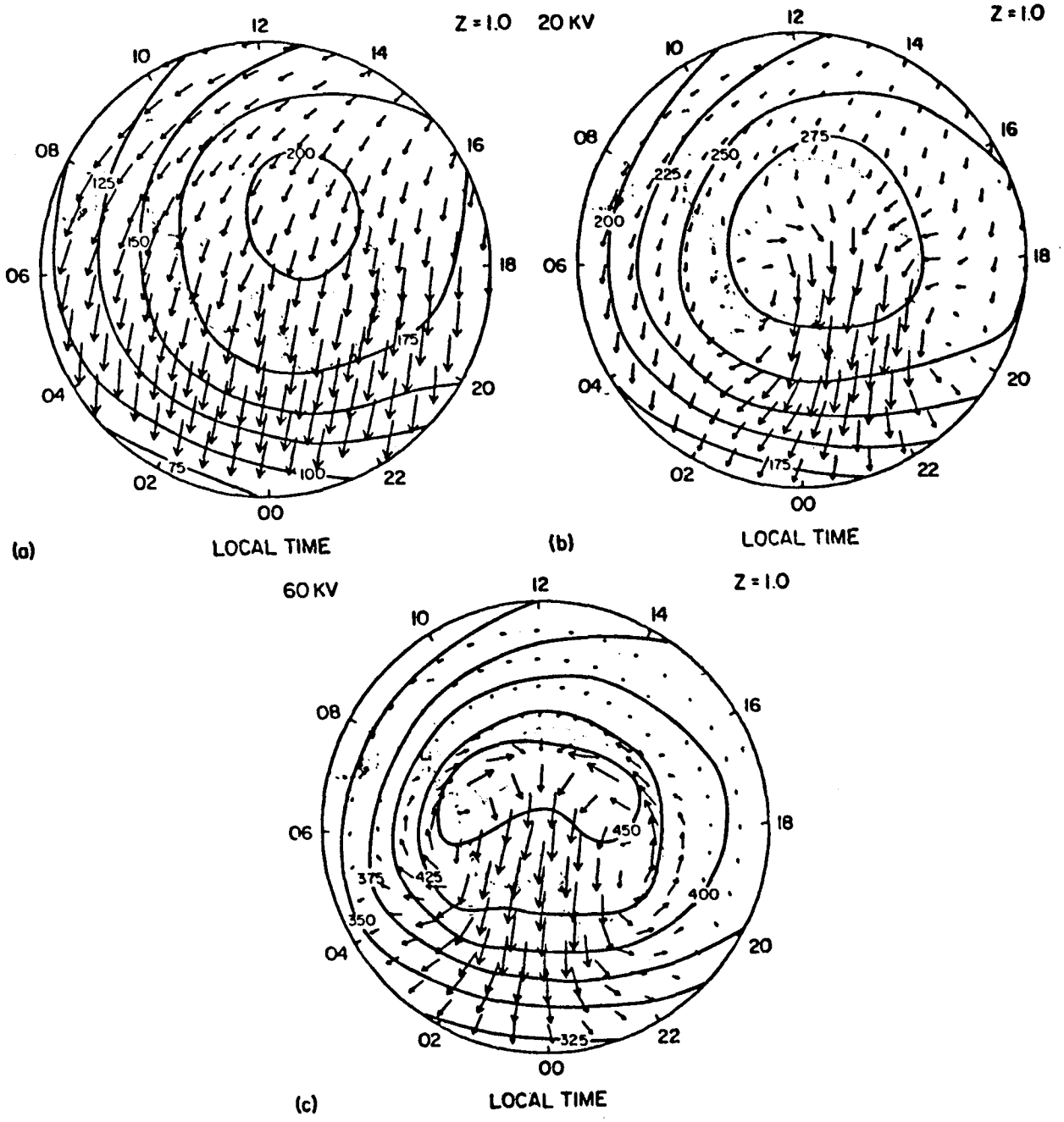

Figure 7. Polar plots giving the direction and magnitude of the calculated southern hemisphere (summer) high-latitude circulation and contours of perturbation temperature (K) along the Z = +1 (300 km) constant-pressure surface at December solstice for (a) solar heating only; (b) solar heating plus magnetospheric convection with a crosstail potential of 20 kV; and (c) solar heating plus magnetospheric convection with a cross-tail potential of 60 kV. The wind speed associated with the maximum arrow is 10 m/s in (a), 200 m/s in (b), and 380 m/s in (c) (Roble et al., 1983).

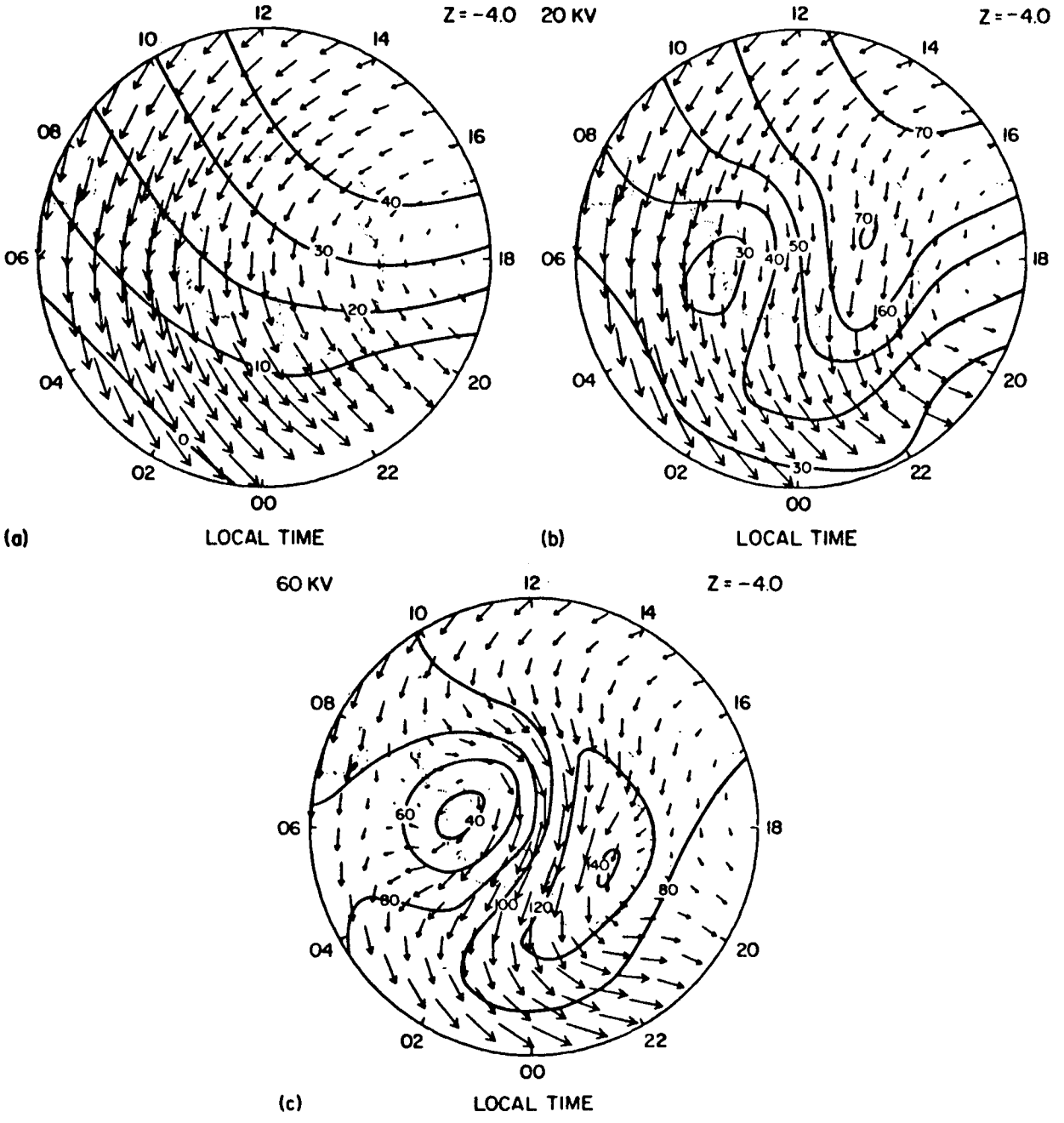

Figure 8. Same as Figure 7, except along the Z = -4 (130 km) constant-pressure surface. The wind speed associated with the maximum arrow is 75 m/s in (a), 77 m/s in (b), and 89 m/s in (c) (Roble et al., 1983)

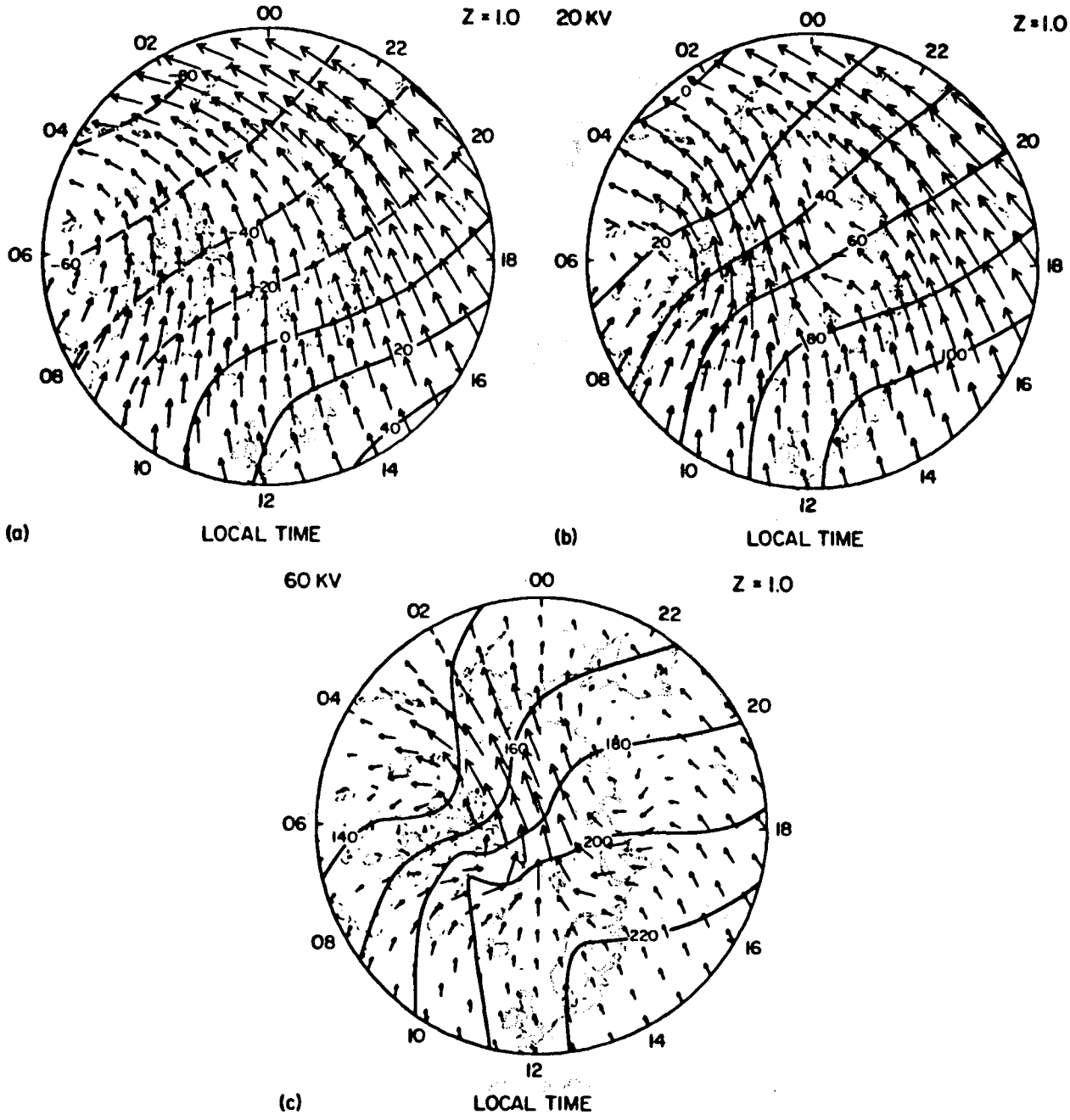

Figure 9. Same caption as in Figure 7 except for northern hemisphere (winter). The wind speed associated with the maximum arrow in 181 m s^{-1} in (a), 200 m s^{-1} in (b), and 339 m s^{-1} in (c) respectively.

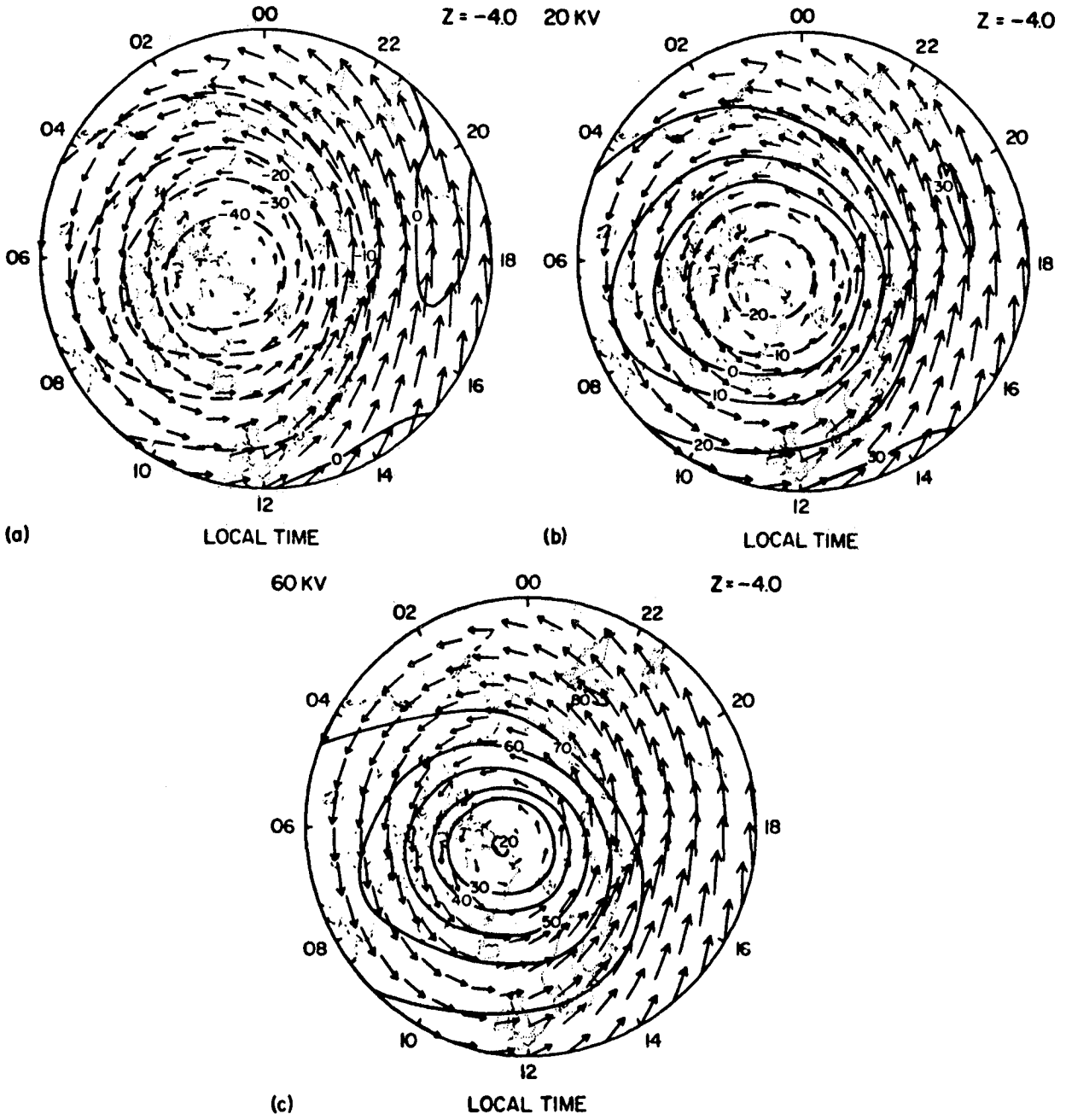

Figure 10. Same caption as in Figure 7 except along the Z = -4 (130 km) constant pressure surface in the Northern Hemisphere (winter). The wind speed associated with the maximum arrow is 108 m s^{-1} in (a), 117 m s^{-1} in (b) and 120 m s^{-1} in (c), respectively.

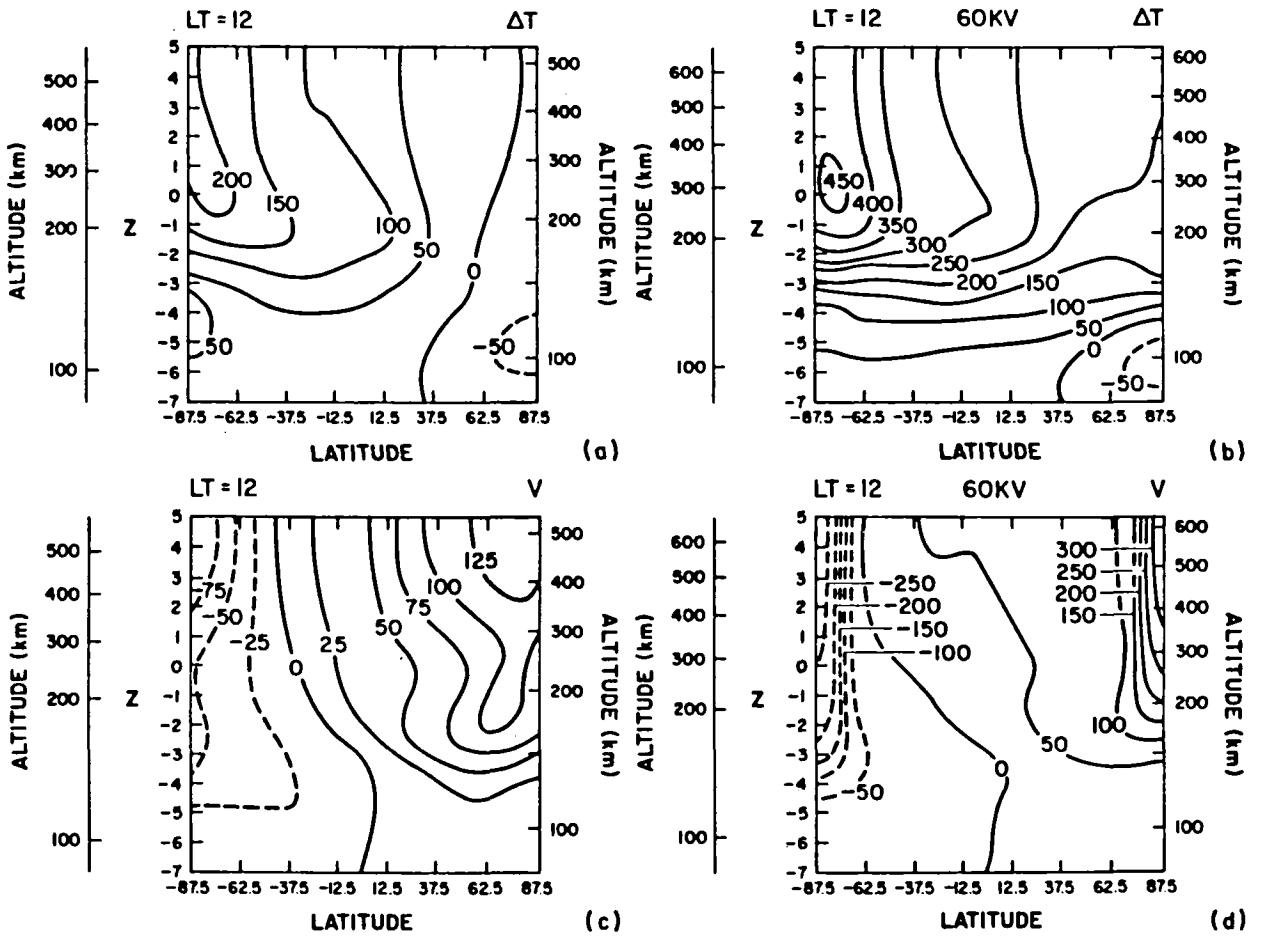

Figure 11. Meridonal cross sections giving contours of the calculated perturbation temperature (K) { (a) and (b) } and meridional wind speed (m s^{-1}, positive northward) { (c) and (d) } , respectively. The local time of the meridional slice is 12.00 L.T. (a) and (c) are the perturbation temperature and meridional wind for the case of solar heating only, and (b) and (d) are the perturbation temperature and meridional wind for the case of solar heating plus magnetospheric convection with a cross-tail potential of 60 kV.

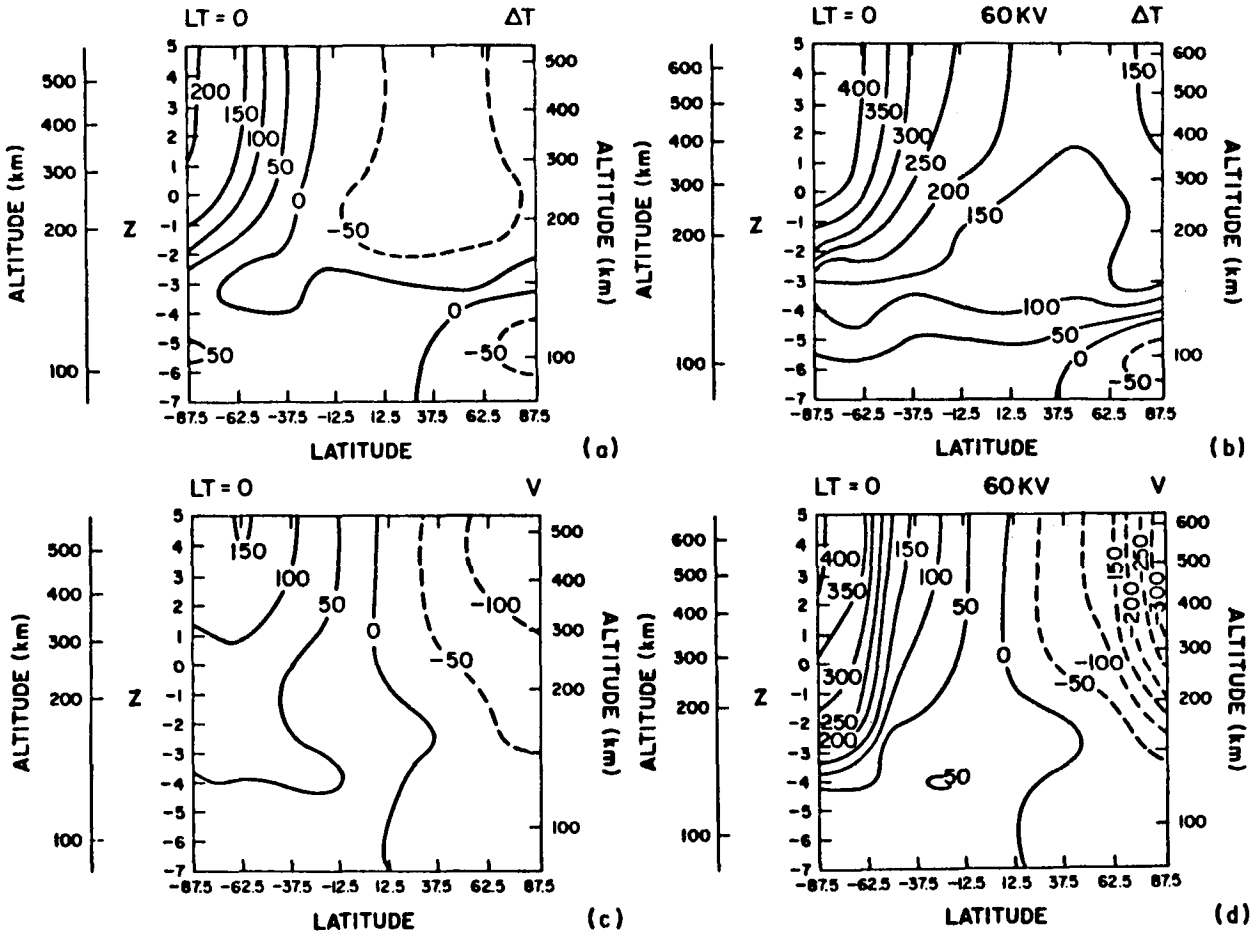

Figure 12. Same caption as Figure 11 except along the 0.00LT meridian.

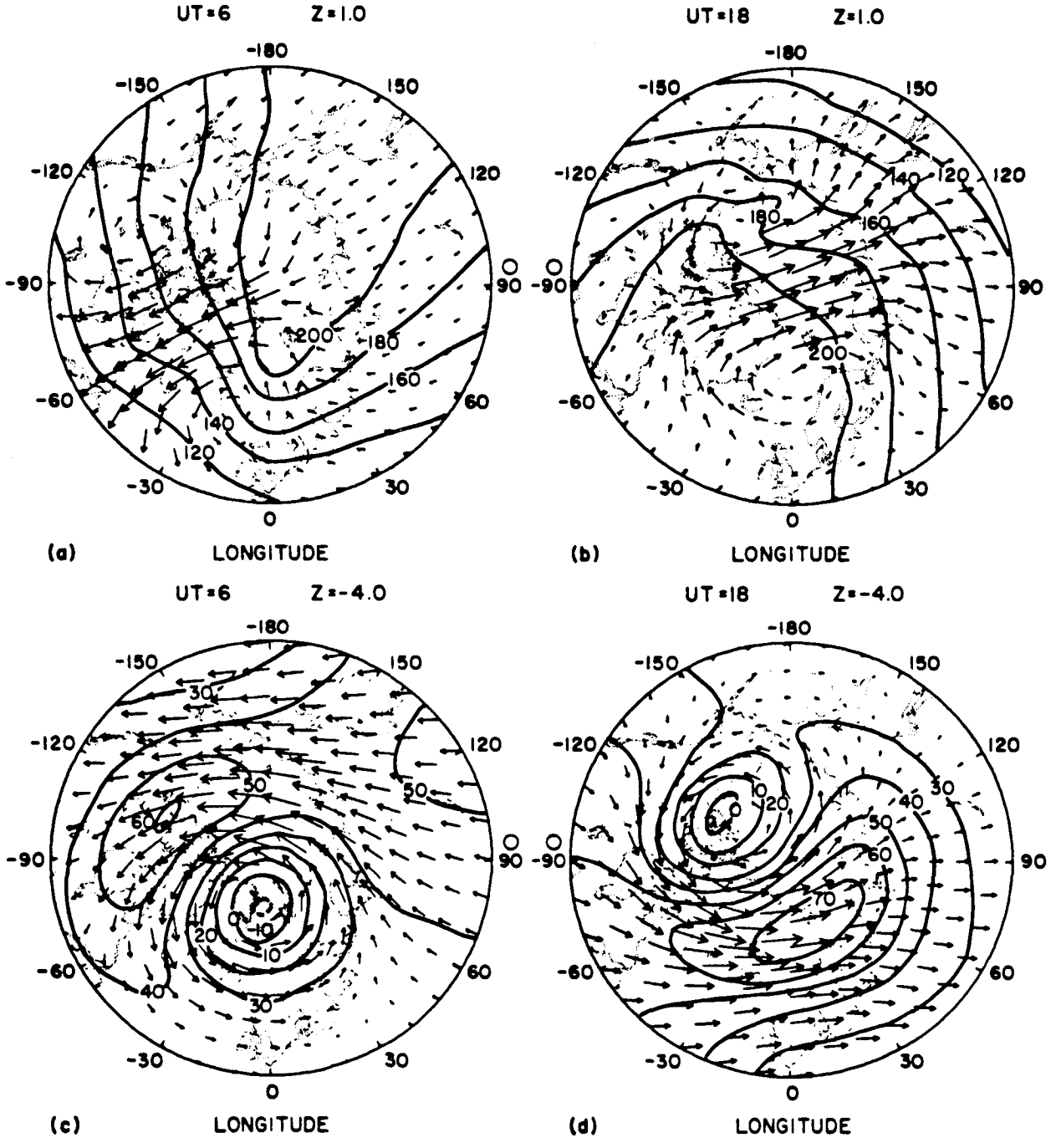

Figure 13. Contours of perturbation temperature (K) along the Z = + 1 (300 km) surface for two universal times, Figure 6a, 0600 UT, and Figure 6b, 1800 UT, and along the Z = -4 (130 km) surface at 0600 UT (Figure 6c) and 1800 UT (Figure 6d) for the case where the geographic and geomagnetic poles are displaced, and the crosstail potential for the magnetospheric convection model is 60 kV. The circulation is indicated by the arrows giving direction, and the length is the magnitude of the winds. The length of the maximum arrow represents 395 m s^{-1} (Figure 6a), 373 m s^{-1} (Figure 6b) 100 m s^{-1} (Figure 6c), and 109 m s^{-1} (Figure 6d), respectively. Local noon is indicated by an open circle on the boundary.

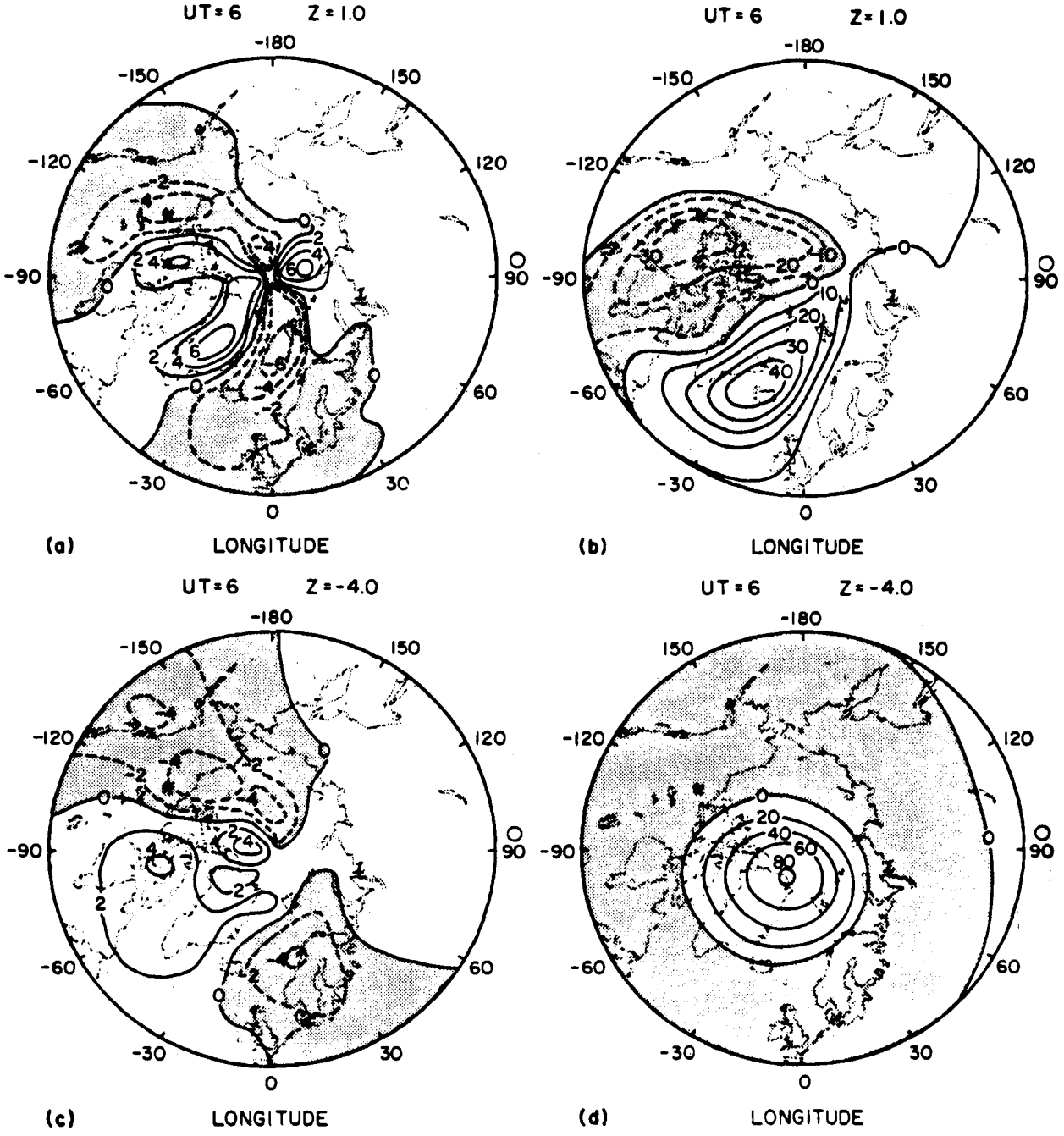

Figure 14. Contours of the calculated divergence and curl of the wind difference field shown in Figures 9b and 9d respectively. Positive contours represent divergence and counterclockwise rotation for the divergent and curl fields, respectively. Units are s^{-1} when these fields are multiplied by 10^{-5} for Figures 10a and 10b and 10^{-6} for Figures 10c and 10d. Local noon is indicated by an open circle on the boundary.

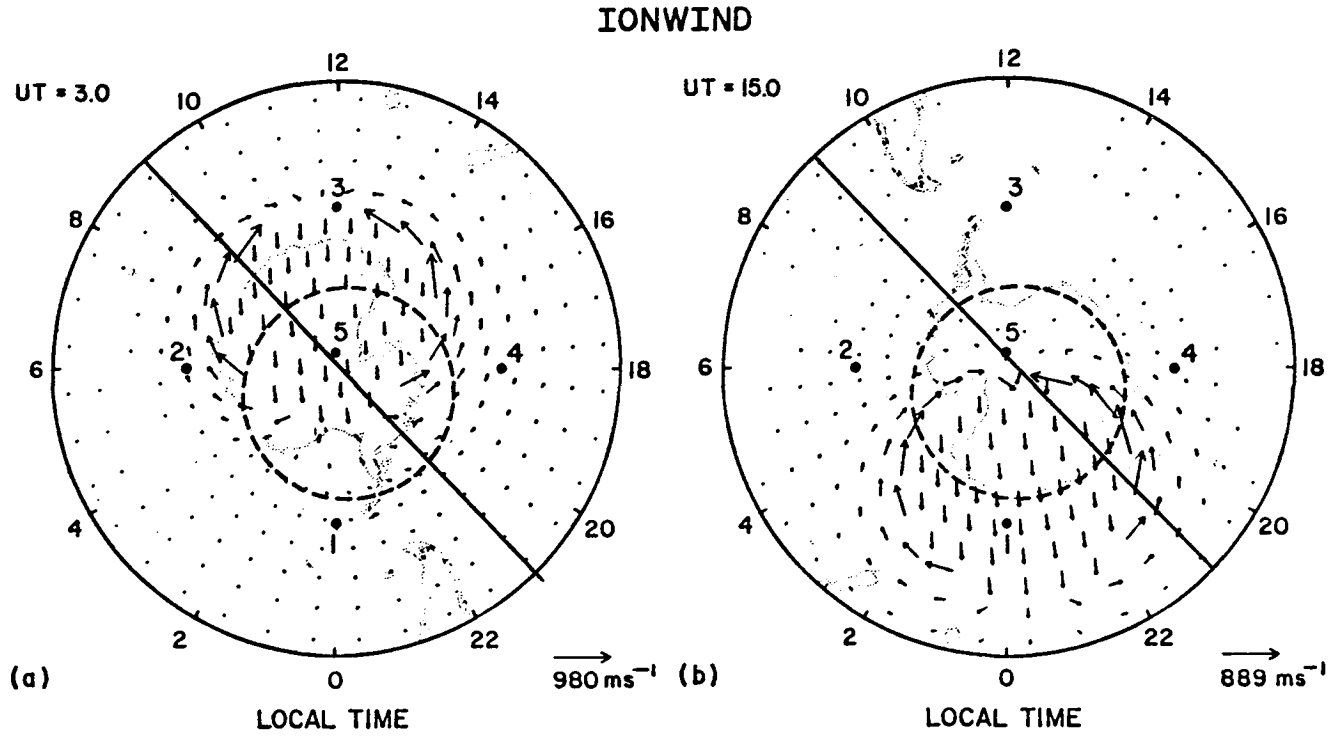

Figure 15. Vectors indicating the magnitude and direction of the ion drift, in the absence of neutral collisions, associated with magnetospheric convection over the southern hemisphere polar cap. The vectors are applied at the upper boundary of the model, and the TGCM calculates the ion drift at different altitudes, considering collisons with neutrals. Displaced geographic and geomagnetic poles are considered. The solid line through the geographic pole shows the geographic position of the satellite track at various universal times.

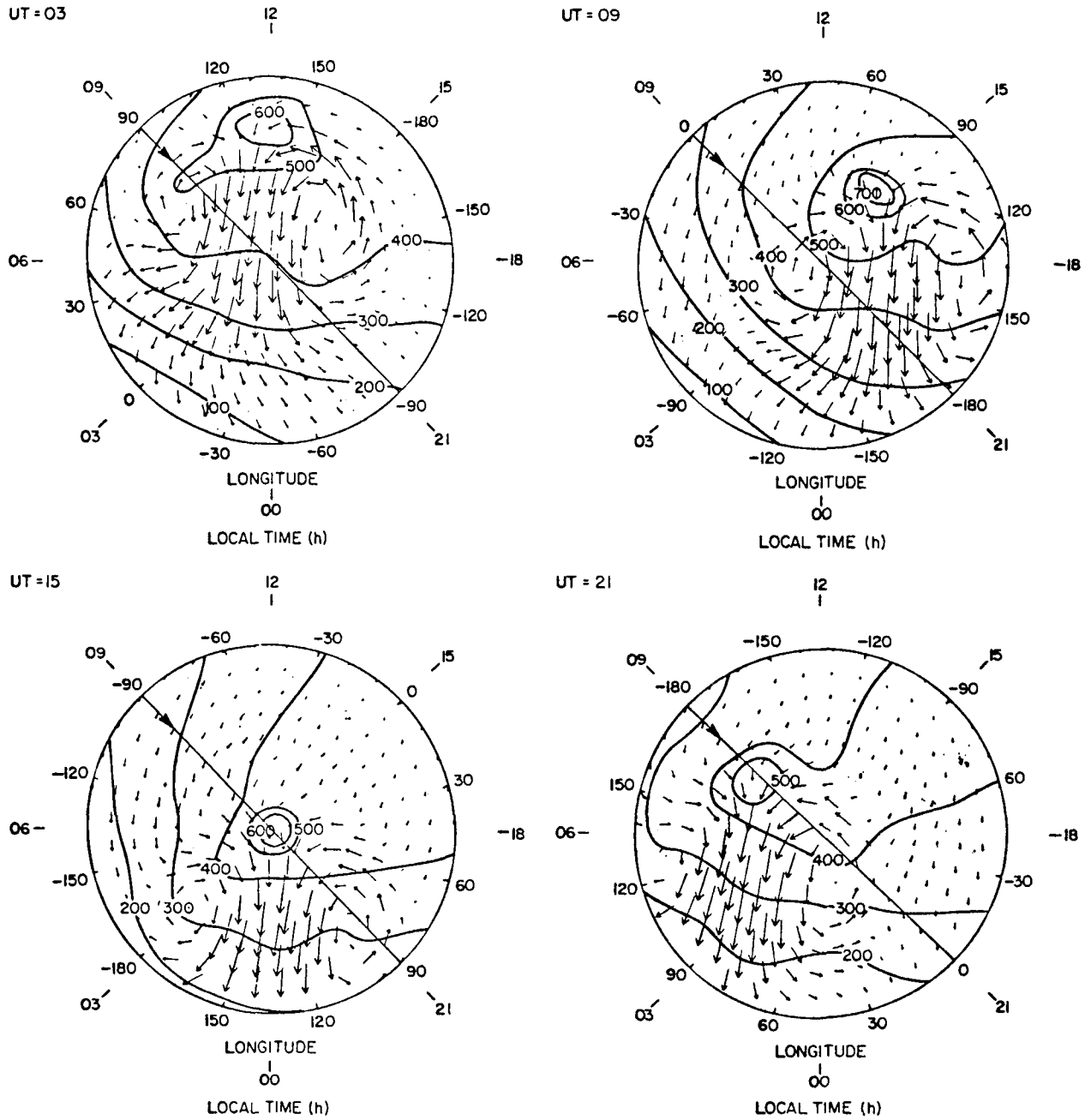

Figure 16. Contours of the TGCM-calculated perturbation temperature (degrees Kelvin) and wind vectors over the southern hemisphere polar cap at four different universal times: (a) 0300 UT, (b) 0900 UT, (c) 1500 UT, and (d) 2100 UT. The winds and perturbation temperature are values along the $Z = +1$ constant-pressure surface (5.4×10^{-5} μbar or 50 Pa) in the TGCM, that is at an altitude of approximately 300 km. The DE 2 satellite track is shown as the solid line in the figure on a 0900-2100 LT pass over the geographic pole. The maximum arrows represent wind velocities of (a) 375 m s^{-1}, (b) 368 m s^{-1}, (c) 404 m s^{-1}, and (d) 409 m s^{-1}, respectively.

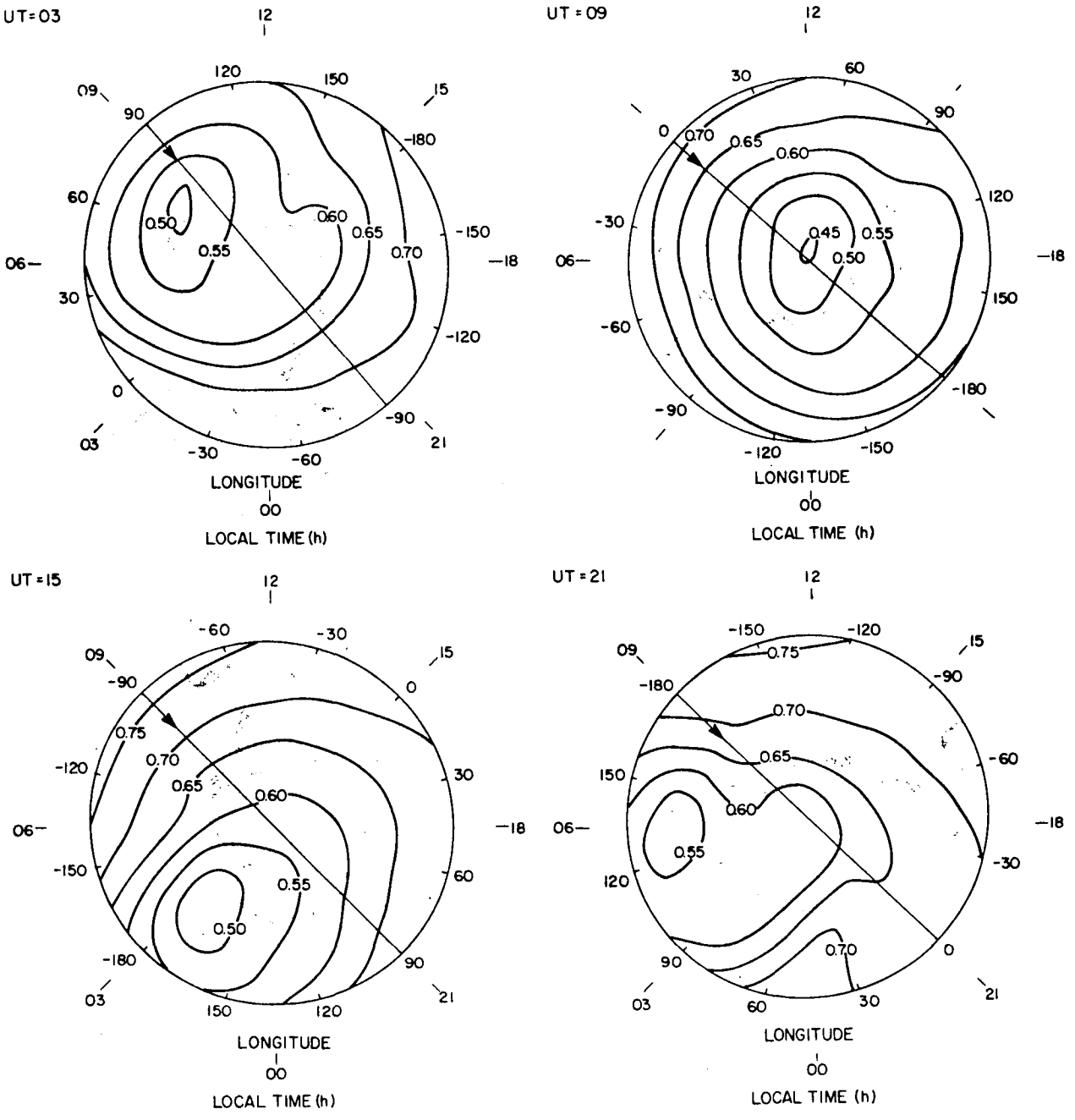

Figure 17. Contours of the TGCM-calculated atomic oxygen mass mixing ratio $\psi(0)$ along the Z = + 1 (300 km) constant-pressure surface over the southern hemisphere polar cap for four different universal times: (a) 0300 UT, (b) 0900 UT, (c) 1500 UT, and (d) 2100 UT.

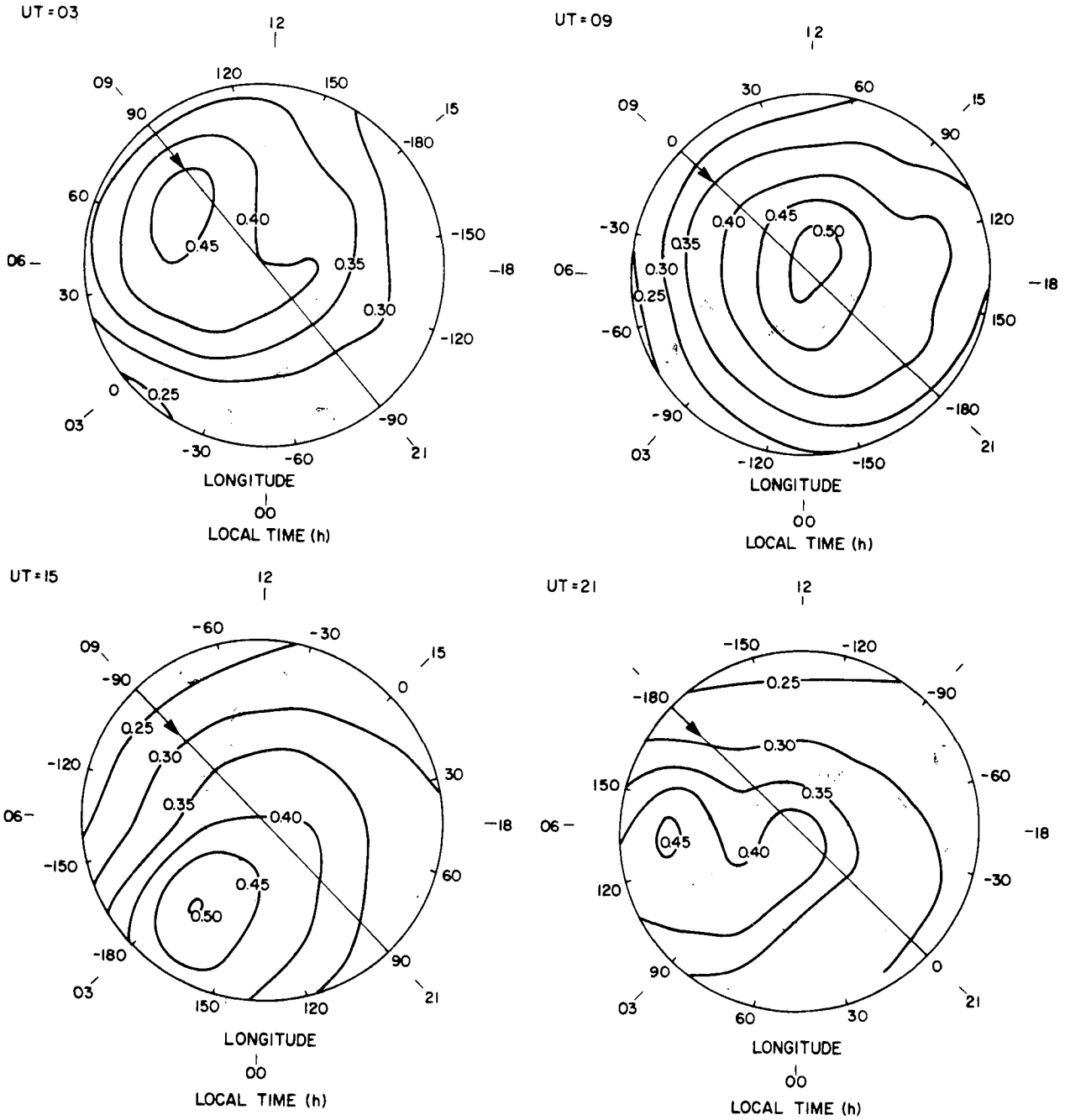

Figure 18. Same as Figure 17, except for the molecular nitrogen mass mixing ration ψ (N_2).

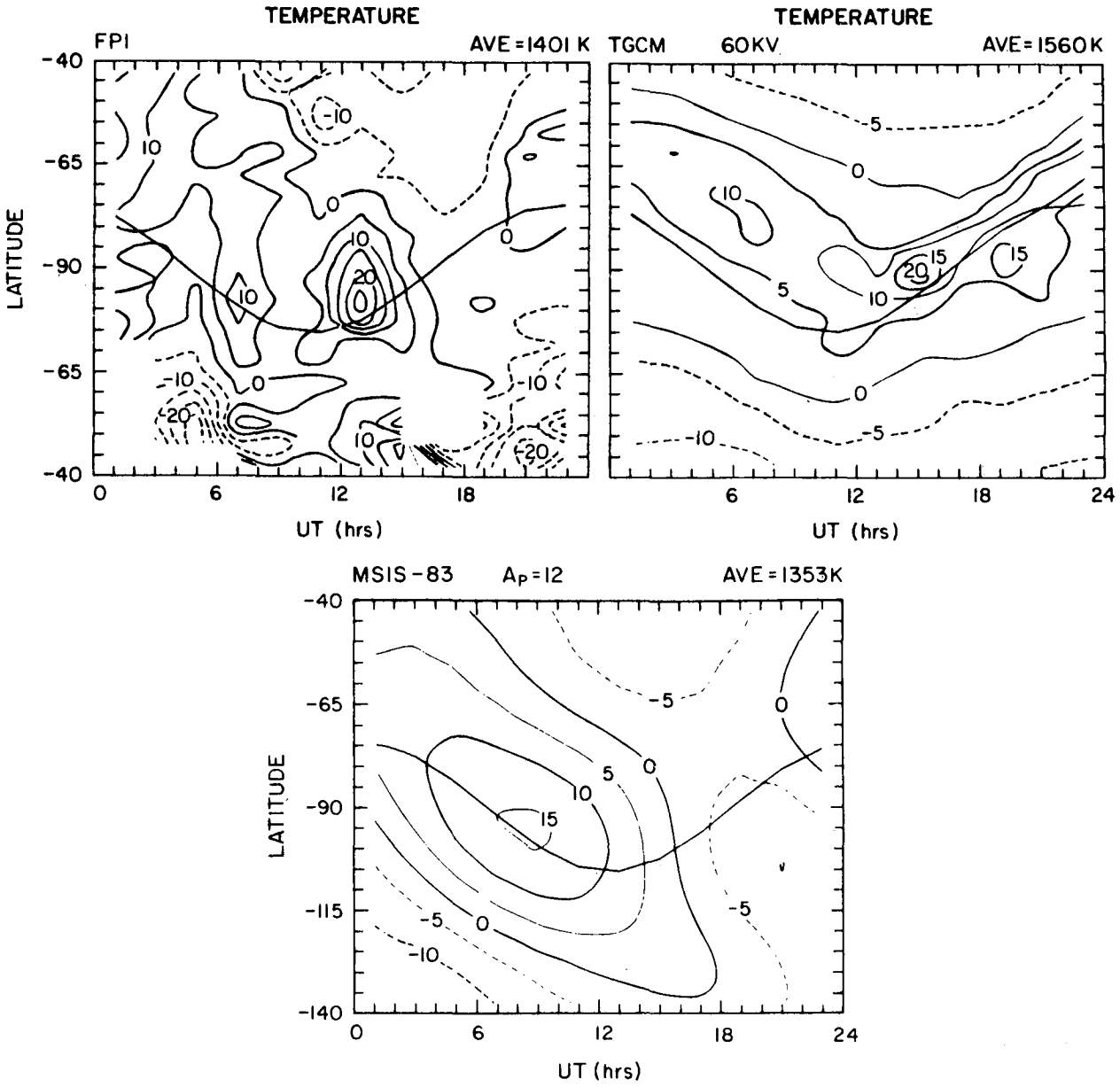

Figure 19. Contours of temperature variation (in percent) from an average value as a function of universal time over the southern hemisphere polar cap. (a) Average of DE 2 FPI measurements during October-November 1981. (b) TGCM model predictions. (c) MSIS-83 model predictions along the satellite track. The average temperature over the latitude-UT grid is indicated in the upper right corner. The solid curve is the geographic position of the south geomagnetic pole as a function of UT. The TGCM model predictions include heating by a magnetospheric cusp and magnetospheric convection with a cross-tail potential of 60 keV. In this figure and all succeeding figures with a similar presentation, data in the top portion of the figure have been obtained at a local solar time of 0900 hours, while data in the bottom part of the figure have been obtained at a local solar time of 2100 hours. This corresponds to the 12-hour local time change as the DE 2 spacecraft crosses the geographic pole in each continuous perigee pass.

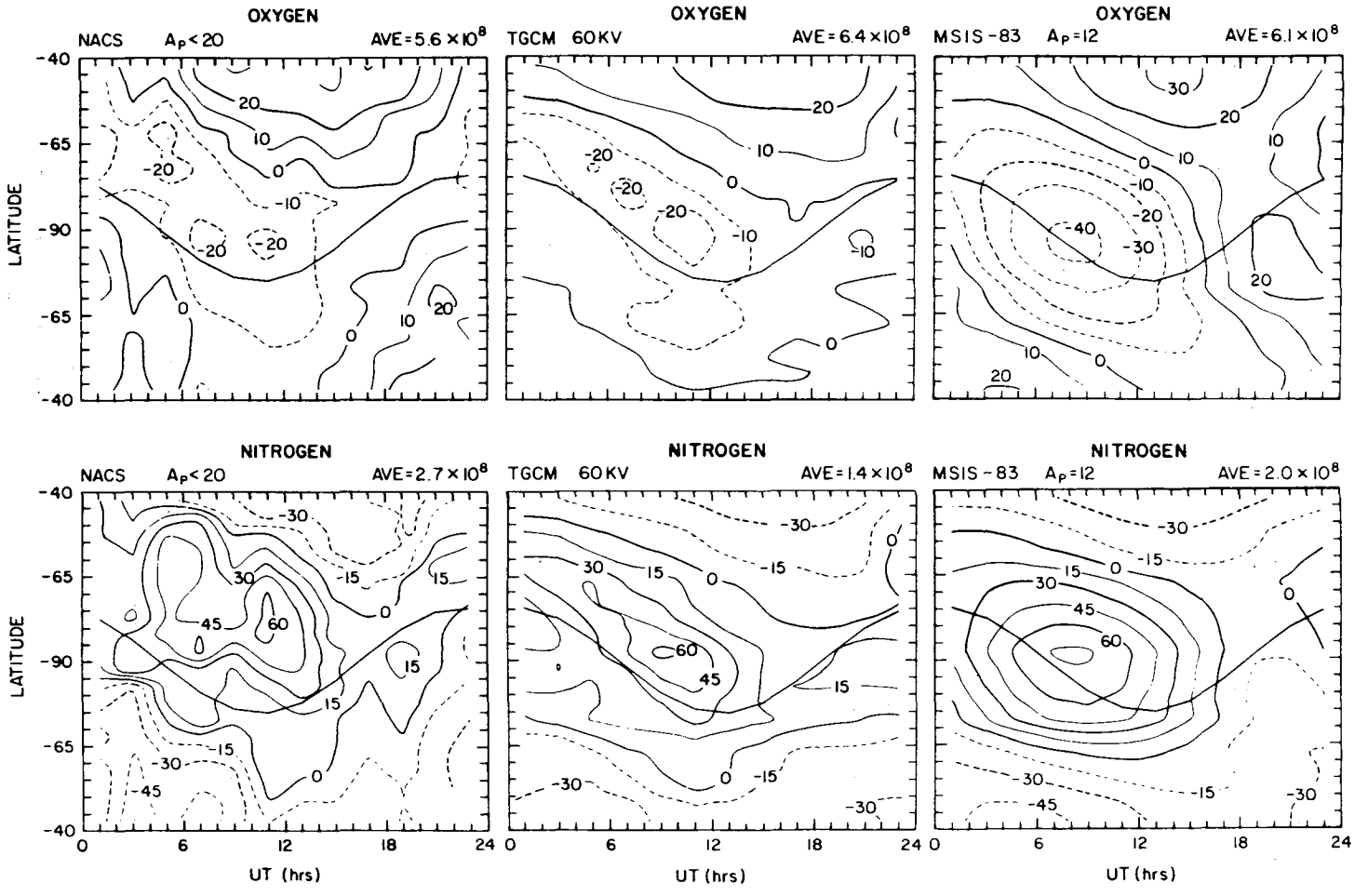

Figure 20. Contours of the percent by which composition departs from an average value as a function of universal time over the southern hemisphere polar cap. (a) Average variation of atomic oxygen and (d) average variation of molecular nitrogen observed by the NACS instrument on board the DE 2 satellite during October-November 1981 for geomagnetic quiet conditions (Ap < 20); (b) TGCM-calculated variation of atomic oxygen; (e) molecular nitrogen; (c) MSIS-83 predicted variation of atomic oxygen; and (f) molecular nitrogen for similar geophysical conditions. The solid curve indicates the projection of the diurnal locus of the south geomagnetic pole on the local time plane of the orbit. The TGCM model includes heating by a magnetospheric cusp and magnetospheric convection with a cross-tail potential of 60 eV.

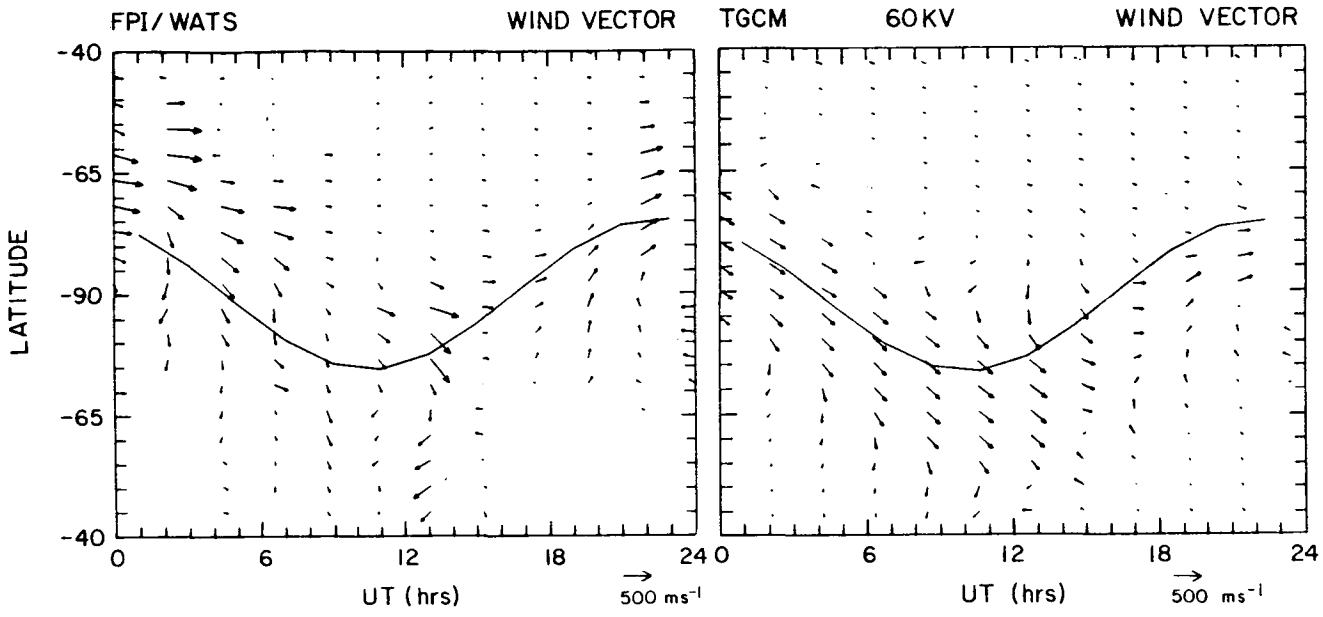

Figure 21. Neutral wind vectors as a function of universal time over the southern hemisphere polar cap. (a) Average of DE 2 FPI/WATS measurements during October-November 1981. (b) TGCM model predictions along the satellite track. The satellite track is from 2100 to 0900 LT (bottom to top of the figure), and the bulk of the arrows indicate a wind directed to the right of the satellite track. The reference arrow for each figure is 500 m s^{-1}. The solid curve indicates the projection of the diurnal locus of the south geomagnetic pole on the local time plane of the orbit. The TGCM model includes heating by a magnetospheric cusp and magnetospheric convection with a cross-tail potential of 60 keV.

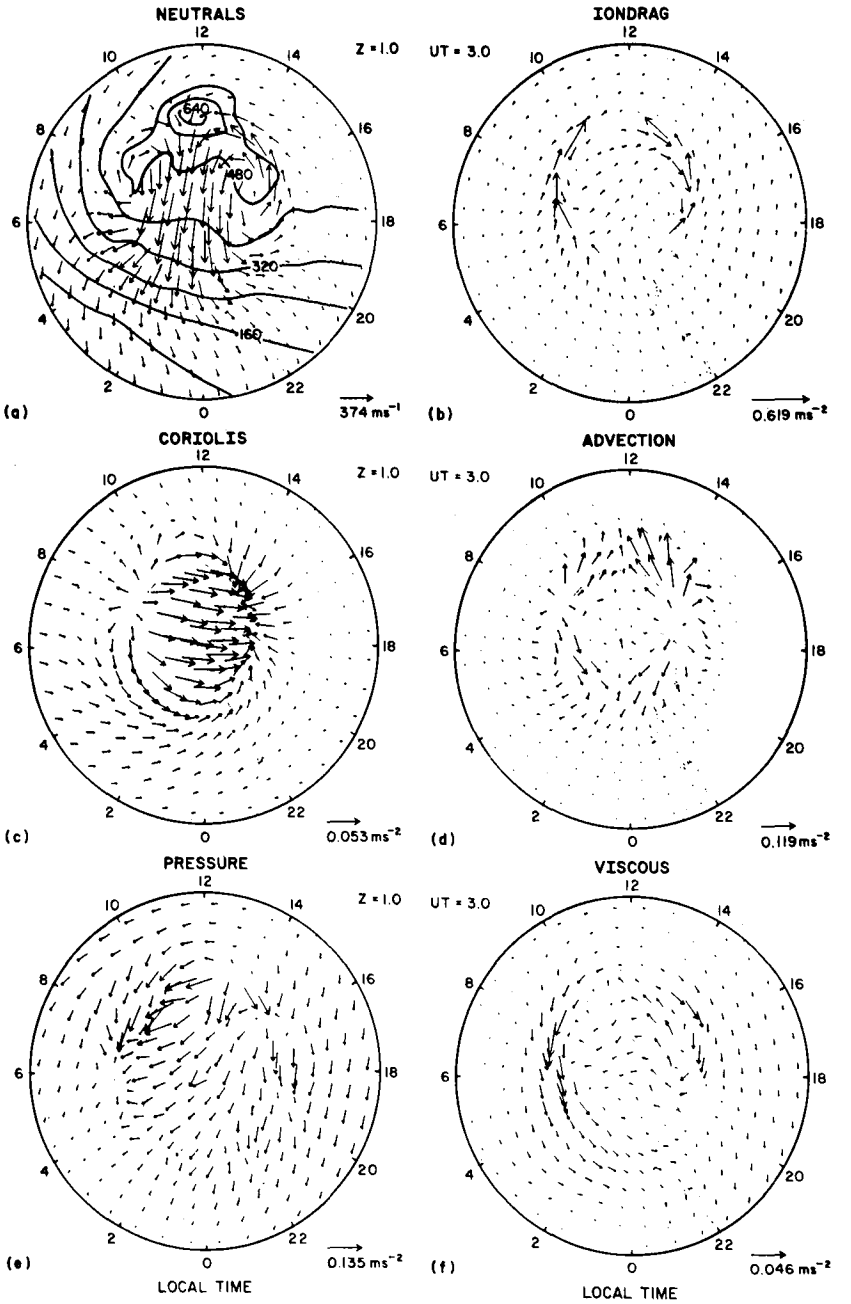

Figure 22. The calculated (a) wind vectors and perturbation temperature contours along the Z = +1 constant-pressure surface over the southern hemisphere polar cap at 0300 UT on October 21, 1981. The maximum arrow in (a) represents a wind velocity of 375 m s^{-1}. The Figures 3b through 3f give vectors of various forces acting on the neutral wind: (b) the ion-drag, (c) Coriolis, (d) advection, (e) pressure, and (f) viscous forces. Note that the length of the maximum arrow represents a different magnitude in each of the figures: (b) 0.62, (c) 0.05, (d) 0.12, (e) 0.14, and (f) 0.05 m s^{-2}.

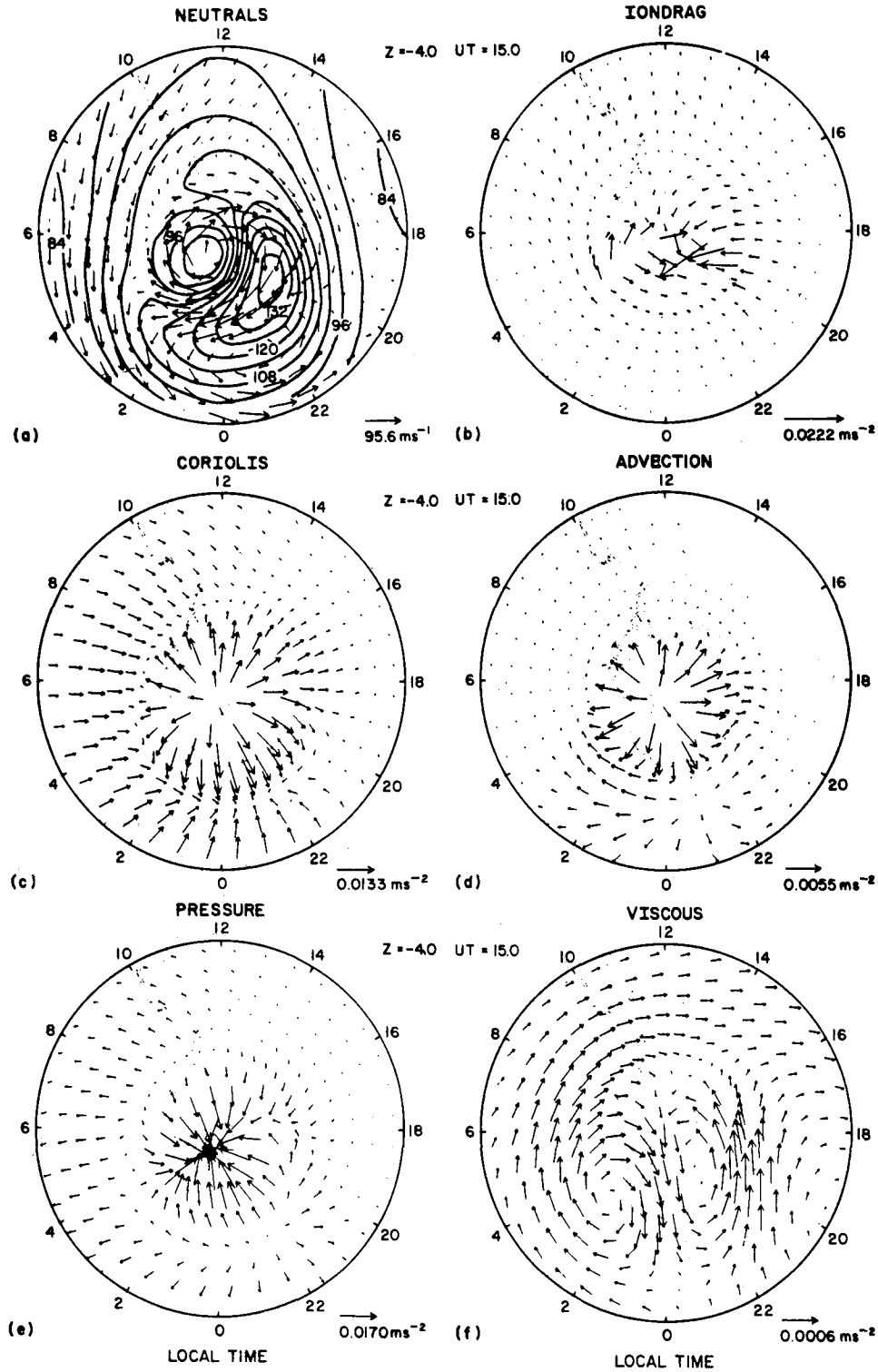

Figure 23. Same as Figure 22, except for the Z = -4.0 constant-pressure surface at 1500 UT. The magnitude of the largest vector in (a) is 98.6 m s^{-1}, (b) 0.022, (c) 0.013, (d) 0.0055, (e) 0.017, and (f) 0.00041 m s^{-2}.

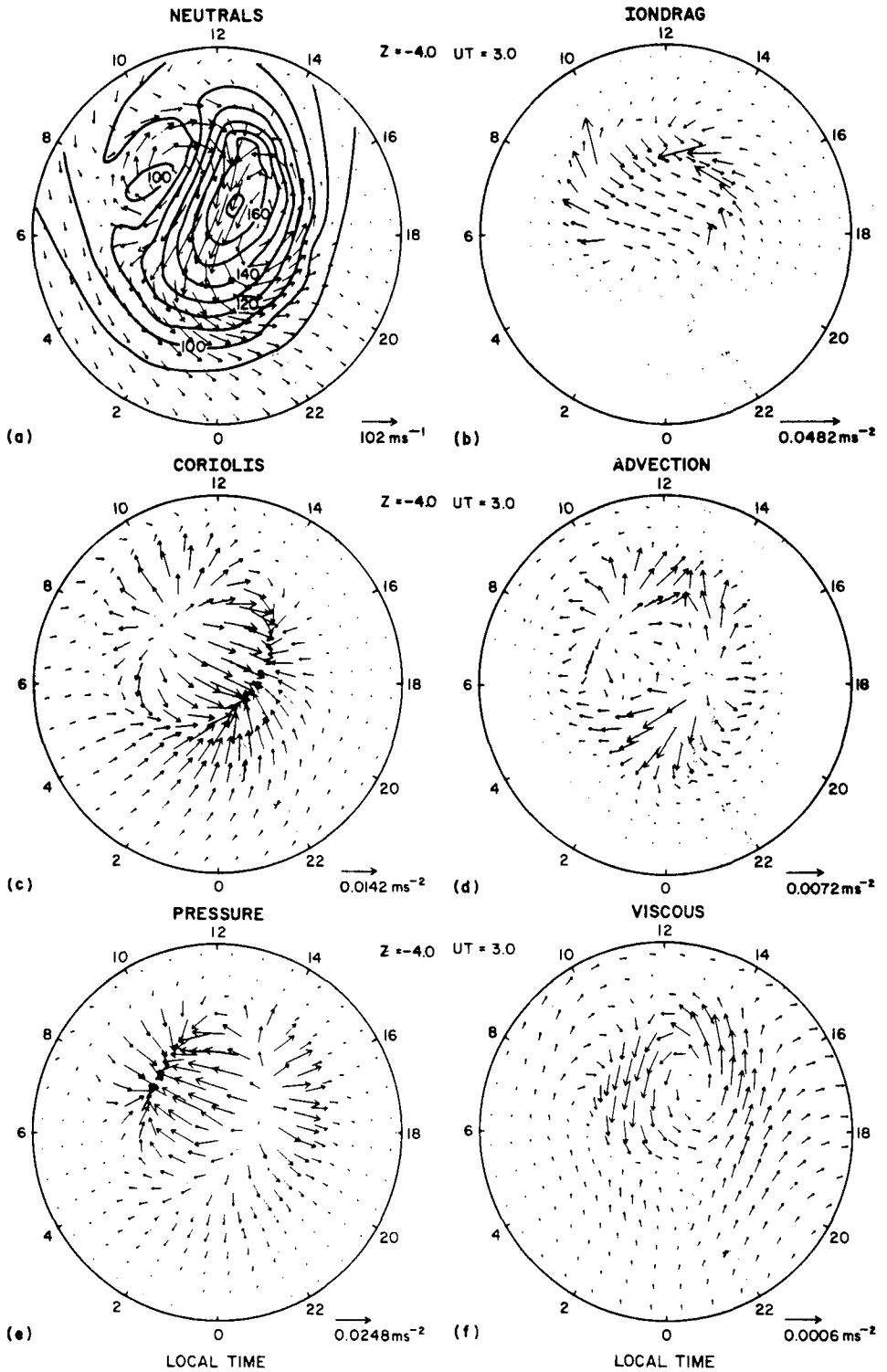

Figure 24. Same as Figure 22, except for the Z = -4.0 constant-pressure surface at 0300 UT. The magnitude of the largest vector in (a) is 102 m s^{-1}, (b) 0.048, (c) 0.014, (d) 0.0072, (e) 0.025, and (f) 0.00057 m s^{-2}.

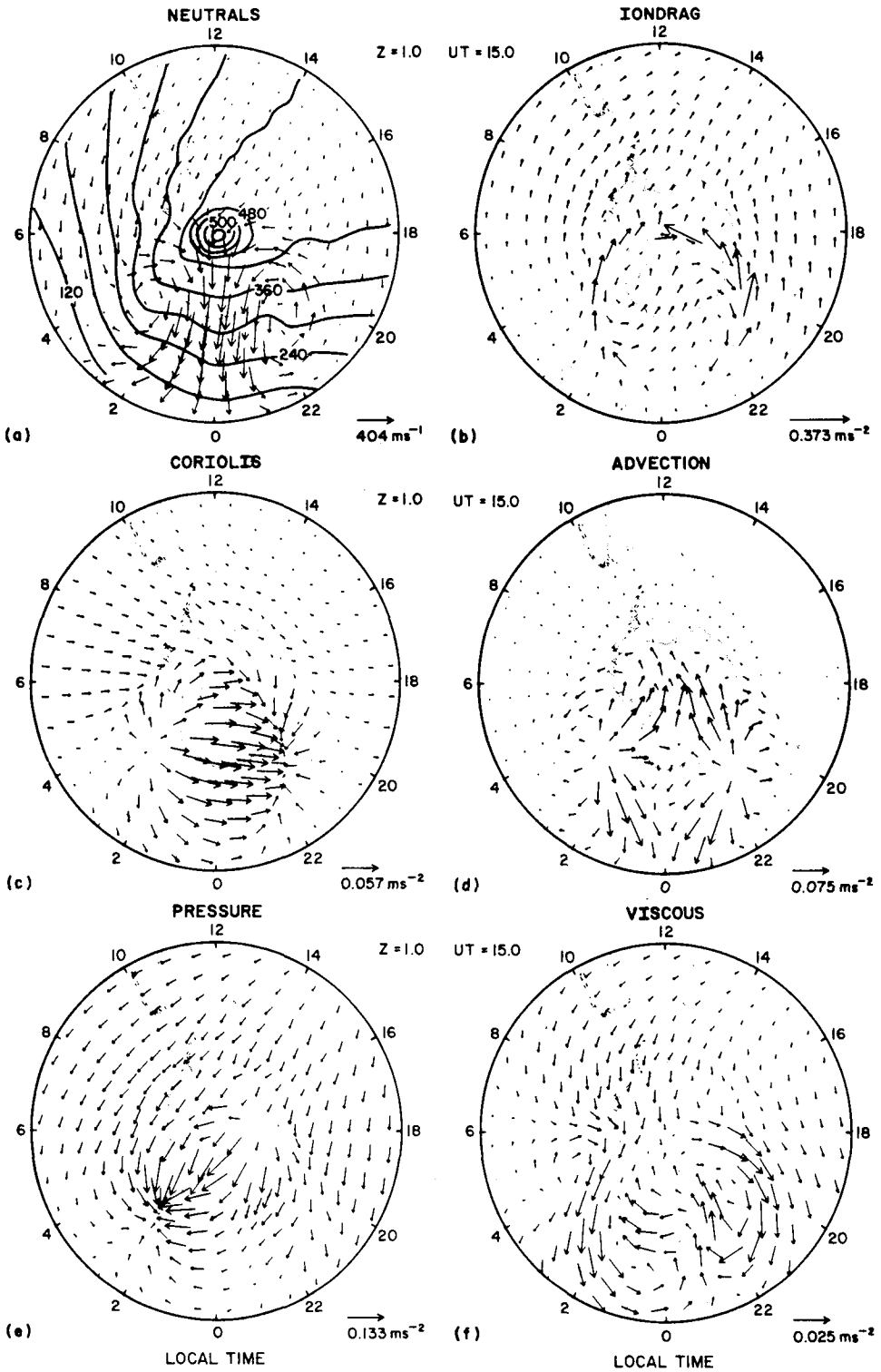

Figure 25. Same as Figure 22, except for 1500 UT. The magnitude of the largest vector in (a) is 405 m s^{-1}, (b) 0.37, (c), 0.06, (d) 0.07, (e) 0.13, and (f) 0.02 m s^{-2}.

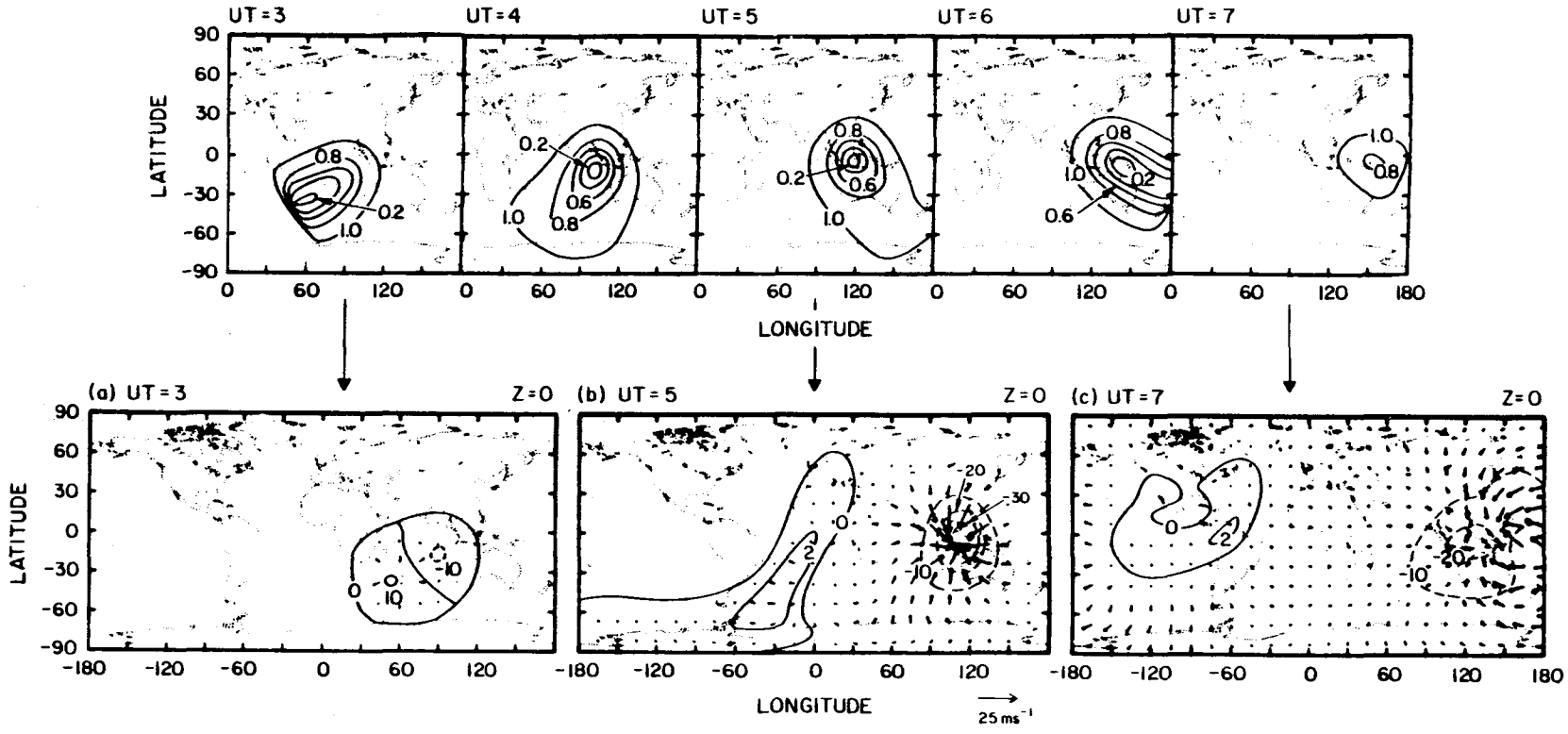

Figure 26. (a) Contours of the calculated eclipse function at 0300, 0400, 0500, 0600, and 0700 UT at 300 km indicating the temporal progression of the eclipse shadow on June 11, 1983. (b) Calculated temperature (degrees Kelvin) and wind (meters per second) difference fields caused by the eclipse shadow at 0300, 0500, and 0700 UT and along the model Z = 0 constant pressure surface at approximately 300 km.

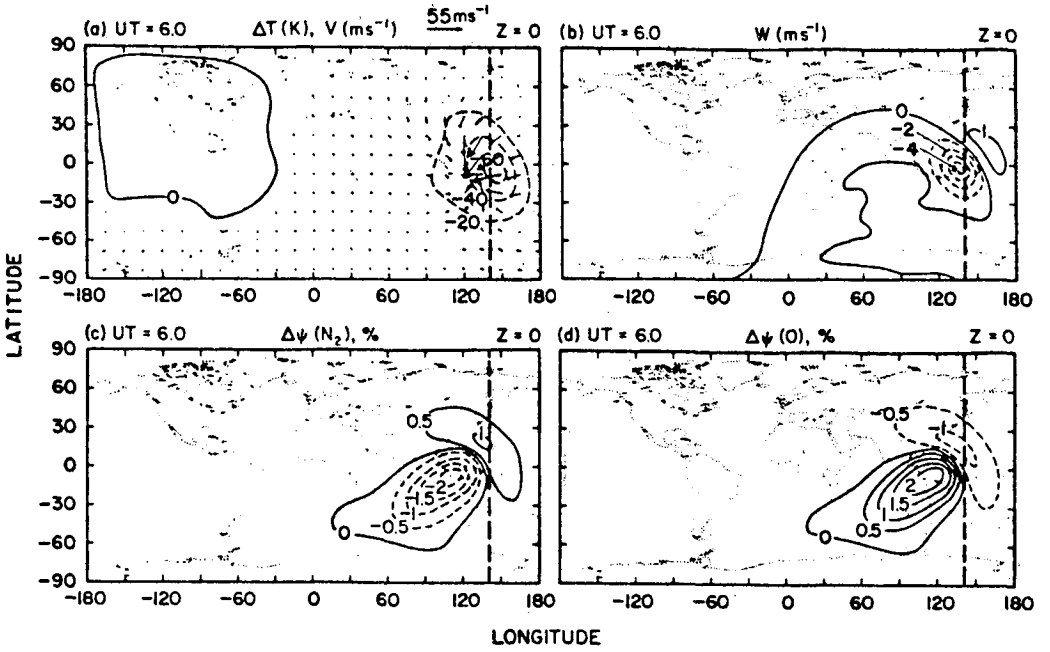

Figure 27. Contours of (a) calculated temperature (degrees Kelvin) and wind (meters per second) difference fields, (b) vertical velocity (meters per second), positive upward, (c) percent deviation of molecular nitrogen mixing ratio, and (d) percent deviation of atomic oxygen mixing ratio at 0600 UT and along the model Z = 0 constant pressure surface near 300 km during June 11, 1983 solar eclipse. The heavy dashed line along the 140°E longitude indicated the cross section of the contours presented in Figure 28.

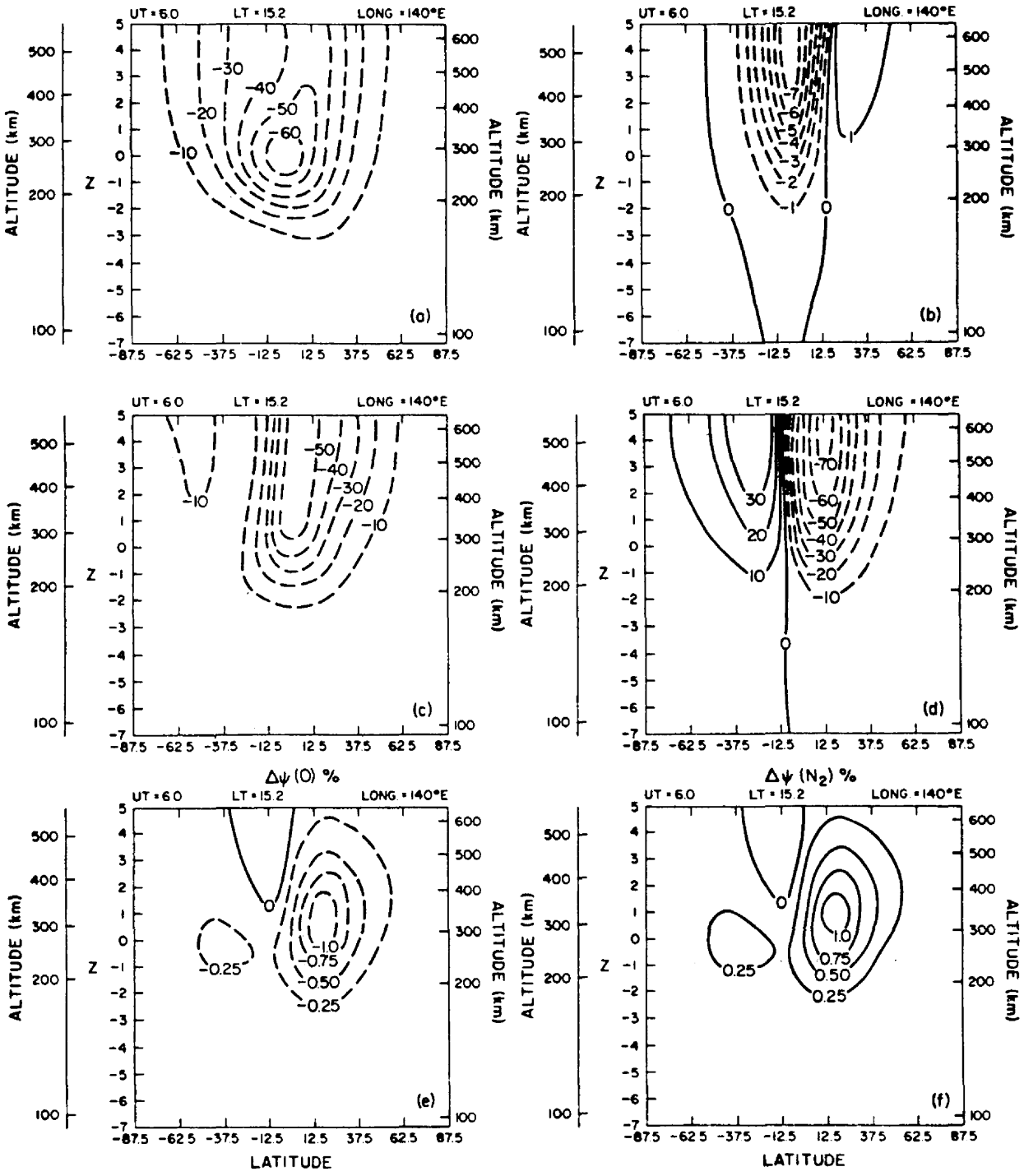

Figure 28. Contours of calculated (a) temperature difference (degrees Kelvin), (b) vertical wind (meters per second), positive upward, (c) zonal wind (meters per second), positive eastward, (d) meridional wind (meters per second), positive northward, (e) percent change of atomic oxygen mixing ratio, and (f) percent change of molecular nitrogen mixing ratio along the 140°E longitudinal slice at 0600 UT during the June 11, 1983 solar eclipse.

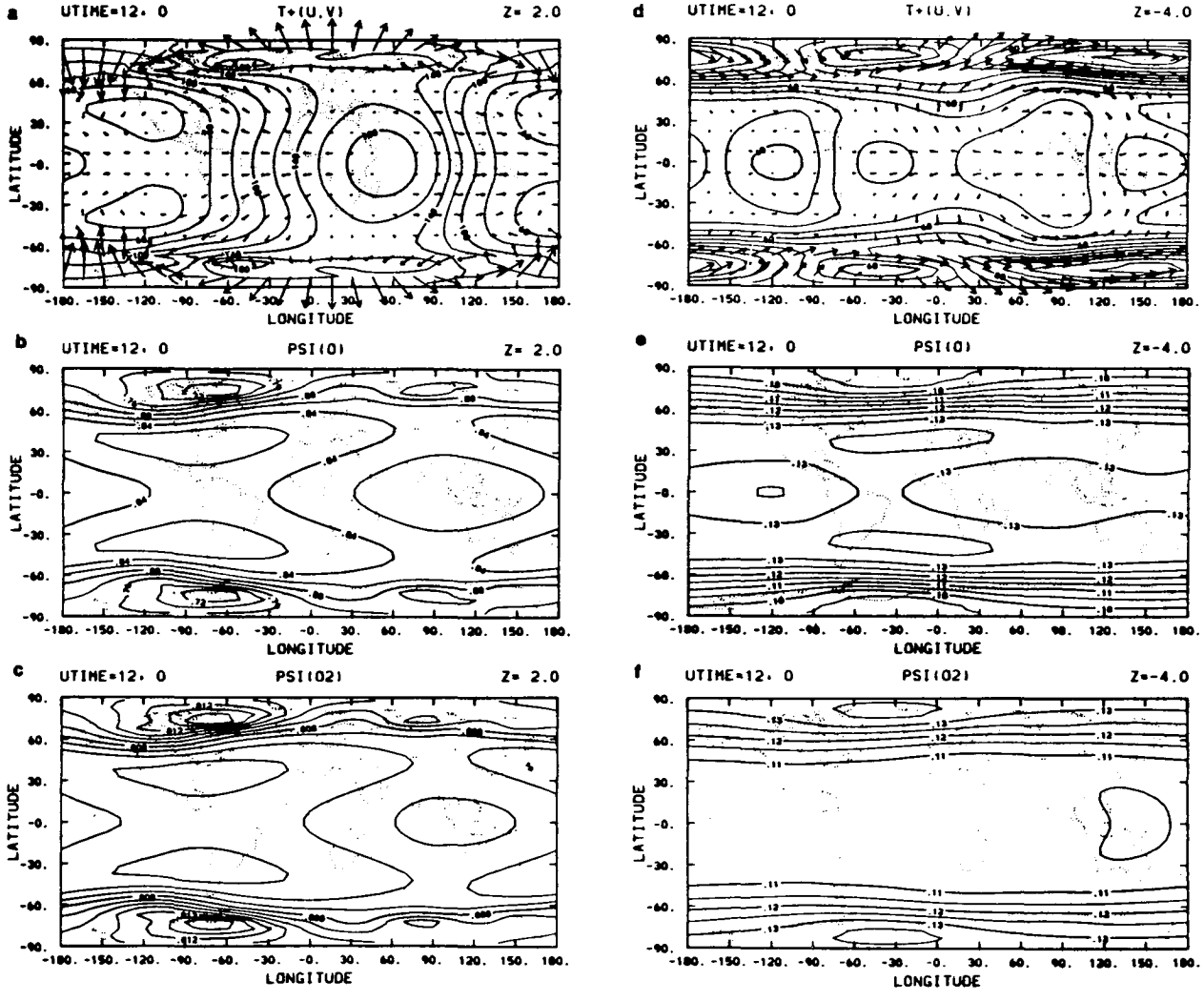

Figure 29. The calculated global circulation, temperature and compositional structure along the Z = +2 (300 km) constant-pressure surface for the case of solar heating plus magnetospheric convection with a cross-tail potential of 60 kV: (a) contours of perturbation temperature (K) and arrows giving wind direction and the length of the wind speed with the maximum arrow representing 336 m s^{-1}; (b) contours of ψ_0; (c) contours of ψ_{02}. The same fields along the Z = -4 (120 km) constant-pressure surface are represented in (d), (e) and (f), respectively. The maximum arrow in (d) represents a wind speed of 79 m/sec.